Drosophila epidermal cells are intrinsically mechanosensitive and modulate nociceptive behavioral outputs

Jiro Yoshino[1,2,3*], Sonali S. Mali[3,4,5*], Claire R. Williams[1,3*], Takeshi Morita[3,6], Chloe E. Emerson[3], Christopher J. Arp[3], Sophie E. Miller[3], Chang Yin[1], Lydia Thé[4], Chikayo Hemmi[2], Mana Motoyoshi[2], Kenichi Ishii[2], Kazuo Emoto[2,7#], Diana M. Bautista[3,4,5#], and Jay Z. Parrish[1,3#]

[1]Department of Biology, University of Washington, Campus Box 351800, Seattle, WA 98195, USA

[2]Department of Biological Sciences, Graduate School of Science, The University of Tokyo, 7-3-1 Hongo, Bunkyo-ku, Tokyo 113-0033 Japan

[3]Division of Education, Marine Biological Laboratory, 7 MBL Street, Woods Hole, MA 02543, USA

[4]Department of Molecular and Cell Biology, University of California, Berkeley, CA 94720, USA

[5]Helen Wills Neuroscience Institute, University of California, Berkeley, CA 94720, USA

[6]Laboratory of Neurogenetics and Behavior, The Rockefeller University, 1230 York Avenue, New York, NY 10065

[7]International Research Center for Neurointelligence (WPI-IRCN), The University of Tokyo, 7-3-1 Hongo, Bunkyo-ku, Tokyo 113-0033 Japan

*These authors contributed equally to this work

[#]Correspondence: jzp2@uw.edu (lead contact), dbautista@berkeley.edu, or emoto@bs.s.u-tokyo.ac.jp

Abstract

Somatosensory neurons (SSNs) that detect and transduce mechanical, thermal, and chemical stimuli densely innervate an animal's skin. However, although epidermal cells provide the first point of contact for sensory stimuli. our understanding of roles that epidermal cells play in SSN function, particularly nociception, remains limited. Here, we show that stimulating *Drosophila* epidermal cells elicits activation of SSNs including nociceptors and triggers a variety of behavior outputs, including avoidance and escape. Further, we find that epidermal cells are intrinsically mechanosensitive and that epidermal mechanically evoked calcium responses require the store-operated calcium channel Orai. Epidermal cell stimulation augments larval responses to acute nociceptive stimuli and promotes prolonged hypersensitivity to subsequent mechanical stimuli. Hence, epidermal cells are key determinants of nociceptive sensitivity and sensitization, acting as primary sensors of noxious stimuli that tune nociceptor output and drive protective behaviors.

42 **Introduction**

The ability to detect tissue-damaging noxious stimuli and mount an escape
44 response is essential for survival. Likewise, prolonged hypersensitivity following injury is an important form of plasticity that protects an animal from further damage. In
46 *Drosophila*, a single class of identified somatosensory neurons (SSNs), class IV dendrite arborization (C4da) neurons, are necessary and sufficient for nociception;
48 inactivating C4da neurons renders larvae insensitive to noxious stimuli whereas activating these neurons drives nocifensive behavior responses (Hwang *et al.*, 2007; Hu
50 *et al.*, 2017; Burgos *et al.*, 2018). A variety of agents that cause tissue damage including UV irradiation and chemical toxins induce long-lasting allodynia and hyperalgesia
52 (Babcock *et al.*, 2009; Boiko *et al.*, 2017), but this damage-induced hypersensitivity develops on a timescale of hours. *Drosophila* also display acute hypersensitivity
54 noxious mechanical stimuli (Hu *et al.*, 2017). However, the cellular and molecular mechanisms underlying mechanical pain hypersensitivity remain enigmatic.

56 Recent studies demonstrate that epidermal cells work in concert with SSNs to transduce noxious and innocuous physical stimuli. For example, epidermal Merkel cells
58 are mechanosensory cells that signal to sensory neurons to mediate touch transduction (Maksimovic *et al.*, 2014; Hoffman *et al.*, 2018). Similarly, keratinocytes are directly
60 activated by noxious thermal and mechanical stimuli and release molecules that modulate nociceptor functions (Chung *et al.*, 2004; Koizumi *et al.*, 2004; Moqrich *et al.*,
62 2005; Mandadi *et al.*, 2009; Liu *et al.*, 2019; Sadler *et al.*, 2020). Furthermore, epidermal cells in invertebrates and vertebrates ensheath nociceptors in mesaxon-like structures
64 (Cauna, 1973; Chalfie and Sulston, 1981; Han *et al.*, 2012; Kim *et al.*, 2012a; O'Brien *et al.*, 2012; Jiang *et al.*, 2019), and these sheaths may serve as sites of epidermis-
66 nociceptor signaling (Yin *et al.*, 2021). Indeed, epidermal ensheathment is required for normal responses to noxious mechanical stimuli in *Drosophila* (Jiang *et al.*, 2019).
68 However, whether epidermal cells are directly activated by noxious stimuli and modulate C4da neuronal activity has not been studied.

70 Here, we examined the capacity of *Drosophila* epidermal cells to drive nociceptor activation and modulate mechanical nociceptive responses. We found that stimulation

of epidermal cells, but no other non-neuronal cell types in the larval body wall evokes activity in a variety of SSNs neurons and triggers nocifensive behavioral responses. Our *in vitro* and *ex vivo* calcium imaging experiments demonstrate that epidermal cells are intrinsically mechanosensitive. Using an unbiased genetic screen, we discovered a role for the store-operated calcium channel Orai, and its activator Stim in epidermal mechanotransduction and mechanical sensitization. Downstream of Stim/Orai activation, epidermal cells evoke nociceptor activation and mechanical hypersensitivity via epidermal vesicular release. Overall, we demonstrate that *Drosophila* epidermis-neuron signaling mediates both the acute detection of noxious mechanical stimuli and a form of prolonged mechanical hypersensitivity.

Results

Stimulation of epidermal cells evokes nocifensive behavior

To identify peripheral non-neuronal cell types that contribute to nociception, we conducted an optogenetic screen for light-evoked nocifensive behavior. First, as a benchmark for comparison we used the light-activated cation channel CsChrimson (Klapoetke *et al.*, 2014) to optogenetically activate nociceptive C4da neurons. Consistent with prior reports (Hwang *et al.*, 2007; Hu *et al.*, 2017), C4da activation triggered nocifensive behaviors including c-bending and rolling in 100% of larvae (Fig. 1A, Fig. 1S1A, Movie S1). Next, we selectively expressed CsChrimson using GAL4 drivers in combination with *elav-GAL80*, which effectively siliences GAL4 expression in larval sensory neurons (Fig. 1S2), to target the six principle non-neuronal cell types within the larval body wall: epidermis, trachea, muscle, hemocytes, oenocytes, and glia (Fig. 1S3, Table S1). We then monitored light-evoked behavioral outputs associated with stimulation of each cell type. We found that optogenetic stimulation of epidermal cells, like C4da neurons, elicited nocifensive c-bending and/or rolling behaviors in 73% of larvae (Fig. 1A, 1S1B), without significantly altering nociceptor morphogenesis (Fig. 1S4). In contrast, stimulation of other body wall cell types elicited a variety of non-nociceptive behavior outputs: for example, muscle stimulation triggered hunching behavior followed by prolonged freezing, whereas glia stimulation reproducibly induced

102 only hunching behavior (Fig. 1S1C-I) (Zimmermann *et al.*, 2009). Thus, epidermal cells
are the only non-neuronal body wall cell type that triggers robust nocifensive behavioral
104 responses.

To further validate the selective ability of body wall epidermal cells to elicit
106 nocifensive behaviors, we examined eight other epidermal drivers in addition to
R38F11-GAL4, which display no expression in sensory neurons and limited non-
108 epidermal cell expression overall (Fig. 1S5). We found that optogenetic stimulation
evoked nocifensive behaviors using each of the eight epidermal driver lines we tested:
110 seven of the lines displayed rolling behavior while all eight displayed c-bending (Fig. 1B,
Fig. 1S6). Although the previously described pan-epidermal *A58-GAL4* driver (Galko
112 and Krasnow, 2004) drove robust nocifensive rolling responses (Fig. 1B, 1S6), *A58-*
GAL4 is expressed broadly in the larval CNS (Fig. 1S7) and stocchastically expressed
114 in sensory neurons (Jiang et al 2014). In contrast, the remaining seven drivers including
R38F11-GAL4 exhibited limited expression aside from epidermal cells, with no
116 detectable expression in nociceptors, other larval SSNs, or peripheral glia, and highly
restricted or undetectable expression in the CNS (Fig. 1S7). Further underscoring the
118 connection between epidermal stimulation and nocifensive responses, the nocifensive
behavioral response with these epidermal drivers correlated with the proportion of
120 epidermal expression (Fig 1B).

We next used thermogenetic stimuluation with the warmth-activated TRP
122 channel dTRPA1 (Hamada *et al.*, 2008) as an independent method of probing
nociceptive responses triggered by epidermal cell activation. On its own, the thermal
124 stimulus (35° C) rarely induced rolling behavior in control larvae bearing *UAS-TRPA1*
alone. In contrast, we found that >75% of larvae expressing TRPA1 in all nociceptors
126 exhibited rolling behavior in response to a thermal stimulus (Fig. 1C). Likewise,
thermogenetic activation of epidermal cells induced robust rolling responses in >75% of
128 larvae, and addition of GAL80 transgenes (*tsh-GAL80 elav-GAL80*) that silenced the
sparse *R38F11-GAL4* VNC expression (Fig. 1S5) had no effect on the rolling frequency
130 (Fig. 1C, Fig. 1S3). Altogether, these results demonstrate that epidermal stimulation
evokes nocifensive responses in *Drosophila*. Of note, prior studies demonstrated that

132 sparse thermogenetic activation of nociceptors (<5 cells) yielded no significant increase in nocifensive rolling whereas activation of >10 cells elicited rolling responses in a
134 majority of larvae (Robertson *et al.*, 2013). Hence, epidermal stimulation likely engages numerous C4da neurons to elicit these behavioral responses.

136 In addition to C4da nociceptors, the epidermis is innervated by a variety of other SSNs including mechanosensory C3da and chordotonal (Cho) neurons and
138 proprioceptive C1da neurons. Whereas direct stimulation of C4da nociceptors principally elicited nocifensive behavioral outputs, epidermal stimulation elicited an array
140 of behaviors in addition to nocifensive responses, including freezing and hunching (Fig. 2A, 2B), behaviors associated with stimulation of C3da and Cho neurons (Zhang *et al.*,
142 2013; Turner *et al.*, 2016). These data suggest that epidermal cells may broadly modulate SSN activity in *Drosophila*.

144 To examine whether different epidermis-evoked behaviors were associated with activation of distinct classes of SSNs, we compared epidermis-evoked and SSN-evoked
146 behaviors. Stimulation of C4da, C3da and Cho neurons elicited distinct behavioral motifs: only C4da neurons elicited rolling behavior; stimulation of C3da and Cho
148 neurons together elicited hunching, C-bending, and backing; stimulation of Cho neurons alone principally elicited hunching and freezing responses (Fig. 2A-2C, 2F). In contrast,
150 optogenetic epidermal stimulation elicited all of these behaviors in a stereotyped sequence, with nocifensive behaviors (c-bending, rolling) preceding non-nociceptive
152 behaviors (backing, freezing) (Fig. 2D, 2F, 2S1). We note that neither the behavioral motifs induced by epidermal or SSN stimulation nor the behavioral sequence induced
154 by epidermal stimulation was recapitulated in effector-only controls (*UAS-CsChrimson* ATR+; Fig. 2S1E), demonstrating that the observed responses were driven by activation
156 of the respective cell types.

We observed three striking differences in behavior evoked by stimulation of
158 epidermal cells versus individual SSNs. First, although rapid, latency to rolling was significantly longer following epidermal stimulation compared to stimulation of C4da
160 (Fig. 2F). Second, the duration of rolling, bending, and backing responses was significantly longer for epidermis versus SSN stimulation (Fig. 2G). Third, backing and

162 freezing behaviors persisted beyond the duration of the light stimulus for epidermis but not SSN stimulation (Fig. 2H). In summary, we find that epidermal stimulation triggers
164 more robust, varied and prolonged behaviors compared to responses from direct stimulation of discrete SSN subtypes.

166

Somatosensory neurons are activated by epidermal stimulation

168 We next asked whether epidermal stimulation activates larval SSNs including C4da, C3da, C1da, and Cho neurons. To test this possibility, we developed a semi-intact larval
170 preparation in which we optogenetically stimulated epidermal cells while simultaneously monitoring calcium responses in axon terminals of SSNs (Fig. 3A). We found that
172 epidermal stimulation triggered rapid and robust calcium transients in nociceptive C4da neurons, responses that were not observed in the absence of ATR or in effector-only
174 controls (Fig. 3B). Epidermal stimulation likewise evoked calcium transients in mechanosensory C3da and Cho neurons, and in proprioceptive C1da neurons (Fig. 3C-
176 3E, 3S1). Hence, epidermal stimulation can broadly modulate activity of larval SSNs.

We next tested the requirement for SSN synaptic transmission in epidermis-
178 evoked behaviors. We stimulated epidermal cells with CsChrimson while blocking SSN neurotransmitter release using tetanus toxin light chain (TnT) (Sweeney *et al.*, 1995).
180 We found that inhibiting C4da or C3da + Cho neurotransmission significantly reduced the frequency and duration of epidermal-evoked rolling and backing behaviors,
182 respectively (Fig. 3E, 3F, 3S2). These data suggest that C4da and C3da/Cho neurons act downstream of epidermal cells to drive behaviors. We note that TnT expression in
184 C4da neurons did not completely block epidermis-evoked nocifensive behaviors, and this likely reflects both incomplete C4da neuron silencing and epidermal activation of
186 other SSNs that promote nociceptive outputs including C3da neurons, C2da neurons, and Cho neurons (Ohyama *et al.*, 2015; Hu *et al.*, 2017; Burgos *et al.*, 2018). Further,
188 silencing C4da or C3da/Cho neurons while stimulating epidermal cells led to an increase in the non-nocifensive behaviors hunching and freezing (Fig. 3E, 3F). These
190 results, along with the observation that rolling behaviors predominate the early behavioral responses to epidermal stimulation (Fig. 2B), suggest that the nervous

192 system prioritizes nocifensive behavioral outputs following epidermal stimulation. These data support a model in which epidermal cells and SSNs are functionally coupled.

194

Epidermal stimulation potentiates nociceptive neurons and behaviors

196 What is the physiological relevance of this functional coupling between epidermal cells and SSNs? To address this question, we compared calcium responses in C4da neurons 198 to simultaneous epidermal and C4da stimulation or C4da stimulation alone. Simultaneous stimulation significantly enhanced the magnitude and duration of calcium 200 responses in C4da axons (Fig. 4A-4D, 4S1). Based on this prolonged calcium response, we hypothesized that simultaneous epidermis and C4da neuron stimulation 202 would yield enhanced nocifensive behavior output. To test this, we optogenetically stimulated C4da neurons and epidermal cells individually or in combination using low 204 intensity CsChrimson activation and monitored larval behavior responses. In this stimulation paradigm, simultaneous epidermal cell and C4da neuron stimulation 206 resulted in rolling in 100% of larvae whereas selective stimulation of C4da neurons or epidermal cells induced rolling in only 63% or 18% of larvae, respectively (Fig. 4E, 4F). 208 Furthermore, simultaneous stimulation elicited a significantly higher number of rolls among responders than stimulation of nociceptors or epidermal cells alone (26.9 rolls 210 for C4da + Epi, 4.9 for C4da, and 5.3 for Epi stimulation; Fig 4G, 4H). Likewise, simultaneous stimulation significantly reduced the latency to the first roll (Fig. 4I) and 212 increased the duration of rolling behaviors (Fig. 4J). We next tested whether this functional coupling extends to mechanical stimuli. We simultaneously presented larvae 214 with a noxious mechanical stimulus and a low intensity optogenetic epidermal stimulus that was insufficient to trigger rolling on its own (0% response rate, n = 200). This 216 concurrent epidermal stimulation significantly increased touch-evoked nocifensive responses, yielding a 91% or 49% increase in rolling responses to 20 mN or 50 mN Von 218 Frey stimulus, respectively (Fig. 4K). We next probed the kinetics of this epidermis-induced mechanical sensitization.

220 When *Drosophila* larvae are presented with two nociceptive mechanical stimuli in succession, they exhibit enhanced behavioral responses to the second stimulus (Hu *et*

222 *al.*, 2017). We hypothesized that selective epidermal stimulation would sensitize larvae
to subsequent nociceptive mechanical stimuli. To test this hypothesis, larvae expressing
224 the warmth-activated calcium-permeable channel dTRPA1 in epidermal cells were
presented with a thermal stimulus, 32º C to activate dTRPA1, followed by a 40 mN
226 mechanical stimulus 10 sec later (Fig. 4L). Indeed, we found that dTRPA1-mediated
epidermal stimulation significantly sensitized larvae to a subsequent mechanical
228 stimulus, increasing the roll probability more than two-fold. In contrast, dTRPA1-
mediated stimulation of C4da neurons did not induce mechanical sensitization, and we
230 confirmed this result with two independent C4da neuron drivers (Fig. 4L). Thus,
activation of epidermal cells but not C4da nociceptors alone induces prolonged
232 sensitization to noxious mechanical stimuli. We next assessed the duration of
sensitization following transient epidermal activation. Thermogenetic epidermal
234 stimulation yielded persistent sensitization that recovered over a timescale of minutes (τ
= 337 sec, Fig. 4M, 4N). The magnitude and duration of mechanical sensitization by
236 thermogenetic epidermal stimulation was remarkably similar to the sensitization evoked
by a prior mechanical stimulus (63% roll probability in response to a second stimulus, τ
238 = 334 sec, Fig. 4N, 4S1B). Altogether our data support a model whereby epidermal cells
are mechanosensitive cells that signal to SSNs to drive acute nocifensive behaviors and
240 prolong mechanical sensitization.

242 ***Epidermal cells are intrinsically mechanosensitive***

Prior studies have shown that vertebrate epidermal cells directly respond to mechanical
244 stimuli (Koizumi *et al.*, 2004; Haeberle *et al.*, 2008; Tsutsumi *et al.*, 2009; Ranade *et al.*,
2014; Woo *et al.*, 2014; Moehring *et al.*, 2018). Therefore, we next assessed whether
246 *Drosophila* epidermal cells are intrinsically mechanosensitive. We developed a protocol
to acutely dissociate epidermal cells and measure the responses of individual
248 GCaMP6s-expressing epidermal cells to mechanical stimuli (Fig. 5A). We found that
radial stretch elicits calcium responses in epidermal cells in a dose-dependent manner.
250 For example, a low 0.5% stretch activated 18% of cells and a subsequent 1% stretch
recruited an additional 10% of stretch-responding cells (Fig. 5B-5D). Overall, 51% of

252 epidermal cells displayed stretch sensitivity (Fig. 5C, 5D). We also found that 43% of epidermal cells responded to hypoosmotic challenge and 35% responded to laminar
254 flow; 19% of epidermal cells responded to both hypoosmotic challenge and laminar flow (Fig. 5S1). Given that dissociated epidermal cells were intrinsically mechanosensitive,
256 we next assessed mechanically evoked responses in a semi-intact body wall preparation (Fig. 5E). We found that 50% of epidermal cells exhibited a robust calcium
258 transient in response to a 25 µm membrane displacement using a glass probe (Fig. 5E-5G, 5S1G). Altogether, these results indicate that *Drosophila* larval epidermal cells are
260 intrinsically mechanosensitive.

262 ***Mechanically evoked epidermal responses rely on store-operated calcium entry***
Our studies demonstrate that, like vertebrate keratinocytes, *Drosophila* epidermal cells
264 exhibit mechanically evoked calcium transients. What is the mechanism of mechanotransduction in these cells? RNA-seq analysis of acutely dissociated epidermal
266 cells revealed expression of more than 20 cation channels, including the mechanosensitive ion channels Piezo, TMEM63, and TMCO (Fig. 6S1). We assessed
268 the epidermal requirements of these channels in mechanical nociception using available RNAi transgenes (Fig. 6A). Our behavioral screen identified one channel, *Orai*, the sole
270 *Drosophila* pore-forming subunit of the Ca^{2+} release-activated Ca^{2+} (CRAC) channel (Feske *et al.*, 2006), that blocked mechanically-evoked nociceptive sensitization without
272 impacting behavioral responses to the first stimulus (Fig. 6A, 6B, 6S2A) or altering nociceptor morphogenesis (Fig. 1S4). Interestingly, our screen uncovered an epidermal
274 role for *Task6*, an orthologue of stretch-sensitive 2-pore potassium channels (Fink *et al.*, 1996), in mechanonociception, as *Task6* RNAi increased nocifensive rolling responses
276 to the initial mechanical stimulus (Fig. 6S2B). Finally, although our RNAi studies did not reveal epidermal requirement for other known mechanosensitive cation channels in
278 mechanonociceptive behaviors, it is possible that multiple channels function redundantly, or that RNAi knockdown was incomplete.

280 To gain insight into mechanically evoked nociceptive sensitization, we focused on probing the role of Orai in epidermal mechanosensory responses. We first asked

282 whether Orai is functional in *Drosophila* epidermal cells. Orai is a store-operated calcium (SOC) channel that is activated by the endoplasmic reticulum (ER)-calcium
284 sensitive molecule, Stim, upon calcium release from ER calcium stores. Thapsigargin (TG) induces calcium release from intracellular stores and thus triggers activation of
286 Orai channels. Indeed, *Drosophila* epidermal cells displayed TG-induced calcium release in the absence of extracellular calcium, followed by calcium influx upon re-
288 addition of extracellular calcium (Fig. 6C). Calcium influx was significantly inhibited by the addition of low nanomolar lanthanum, consistent with the high sensitivity of Orai
290 channels to lanthanides (Fig. 6S2C). This characteristic store operated calcium entry (SOCE) response was significantly reduced by epidermis-specific *Stim* or *Orai* RNAi
292 knockdown (Fig. 6S2D-F). Consistent with a key role for SOCE in mechanotransduction, we found that radial stretch induced both calcium release from
294 intracellular stores in the absense of extracellular calcium and influx upon calcium re-addition. While both store release and calcium influx constitute the calcium response to
296 stretch, in 69% of cells, calcium due to store release exceeded that of calcium re-entry (Fig. 6E). Consistent with this observation, depletion of intracellular stores and inhibition
298 of calcium re-entry reduced the number of stretch sensitve cells by 61% (stretch non-responsive cells in control = 49% vs. store depleted = 80%) and 30% (stretch non-
300 responsive cells in control = 49% vs. La^{3+} = 64%; Fig. 6F-G), respectively. Given that Stim and Orai mediate SOCE in epidermal cells and that stretch evokes SOCE, we
302 investigated requirements for epidermal Stim and Orai in mechanically evoked calcium responses. RNAi knockdown of either *Stim* or *Orai* significantly reduced the fraction of
304 stretch-responsive epidermal cells (RNAi control = 48%, *Stim* RNAi = 22%, *Orai* RNAi = 24%; Fig. 6H-I), with *Stim* or *Orai* RNAi preferentially attenuating stretch evoked
306 responses to larger magnitude stretch stimuli. We also found that human keratinocytes display dose-dependent stretch evoked calcium responses, though they respond to
308 higher magnitudes of stretch than *Drosophila* epidermal cells (Fig. 6J). Like *Drosophila*, both store release and calcium influx contribute to stretch evoked calcium responses in
310 human keratinocytes (Fig. 6K).

Two hallmarks of Stim and Orai-mediated SOCE are steep inward rectification, with larger currents at hyperpolarizing potentials, and highly cooperative Orai activation by Stim (Hoover and Lewis, 2011). Since Stim and Orai mediate mechanical responses of epidermal cells *in vitro*, we predicted that increasing the calcium driving force through Orai activity by either hyperpolarizing epidermal cells or by activating additional Orai channels via *Stim* overexpression would enhance behavioral responses to mechanical stimuli. Indeed, we found that hyperpolarizing epidermal cells with the light-activated anion channelrhodopsin GtACR1 (Mohammad *et al.*, 2017) increased behavioral responses to mechanical stimuli (Fig. 6L). In addition, overexpressing *Stim* in epidermal cells significantly enhanced nocifensive behavioral responses to mechanical stimuli (Fig. 6M). Altogether, these results demonstrate that mechanically evoked responses of epidermal cells and the resulting nocifensive behavior outputs require store-operated calcium entry.

How might mechanically evoked calcium entry in epidermal cells drive nociceptor activation and behavior? Stim/Orai-mediated calcium entry contributes to exocytosis in a variety of cell types, including neurons and immune cells (Pores-Fernando and Zweifach, 2009; Ashmole *et al.*, 2012; Maneshi *et al.*, 2020; Chanaday *et al.*, 2021; Ramesh *et al.*, 2021). Therefore, we investigated the contribution of epidermal exocytosis in nociceptive sensitization with the temperature-sensitive dynamin mutant *shibire*^{ts} (*shi*^{ts}) to inducibly block vesicle recycling, as this treatment rapidly and potently blocks neurotransmitter release (Koenig *et al.*, 1983) and we found that acute epidermal dynamin inactivation using *UAS-shi*^{ts} had no discernable effect on nociceptor morphogenesis (Fig. 1S4). In this paradigm, larvae expressing *shi*^{ts} in epidermal cells, but not control larvae, exhibited significant attenuation of mechanically evoked nociceptive sensitization following pre-incubation at the non-permissive temperature (Fig. 6N). In contrast, both genotypes exhibited comparable responses to a mechanical stimulus at the permissive temperature (25° C) and to the first mechanical stimulus following pre-incubation at the non-permissive temperature (30° C). Taken together, these results are consistent with a model in which mechanical stimuli induce calcium influx and vesicular release from epidermal cells, which in turn activates nociceptors to

induce acute nocifensive behaviors and prolonged sensitization (Fig. 6O). Although our
342 RNA-seq analysis of epidermal cells did not reveal expression of neurotransmitter biosynthesis genes, epidermal cells express a large repertoire of genes involved in
344 vesicular release as well as several neuropeptide genes, providing an entrypoint to defining the molecules involved in epidermis-SSN communication.

346

Discussion

348 In this study, we have shown an essential role for *Drosophila* epidermal cells in escape responses to noxious mechanical stimuli. Activation of epidermal cells acutely
350 activates SSNs to induce an array of behavioral outputs and mechanical sensitization. This epidermal potentiation persists for minutes to promote a prolonged, but reversible,
352 mechanical hypersensitivity that may protect from further insult. This is distinct from previously described forms of neuropathic thermal and mechanical hypersensitivity in
354 *Drosophila* which are induced by tissue damage and chemotherapuetic agents, respectively, emerge on a timescale of hours, and are long-lasting (Babcock *et al.*,
356 2009; Boiko *et al.*, 2017; Khuong *et al.*, 2019). In the mammalian somatosensory system, a variety of inflammatory mediators have been shown to activate TRPA1 in
358 neurons to promote mechanical hypersensitivity (Bautista *et al.*, 2006); however, the molecular force transducers that mediate mechanical pain are unknown. In contrast, in
360 the *Drosophila* somatosensory system, *Ppk1*/*Ppk26*, *Piezo*, and *Trpa1* are key transducers of mechanonociception (Zhong *et al.*, 2010; Kim *et al.*, 2012b; Gorczyca *et*
362 *al.*, 2014; Guo *et al.*, 2014; Mauthner *et al.*, 2014). Prolonged sensitization to noxious mechanical stimuli plays an important protective role in an organism's survival; yet the
364 mechanisms of mechanical sensitization of *Drosophila* nociceptors were unknown.

We demonstrate a new role for SOCE signaling in both *Drosophila* and human
366 epidermal cell mechanotransduction. While short-term sensitization is beneficial to survival, a key hallmark of pathological pain is prolonged and persistent mechanical
368 hypersensitivity; whether deregulation of this mechanism of epidermis-evoked short-term sensitization contributes to pathological pain remains to be determined. Overall,
370 we identified a mechanism that does not impact acute nociception but selectively

regulates mechanical sensitization. These findings highlight Stim/Orai signaling as a
372 new avenue for understanding mechanical pain.

This work has opened several new directions for future studies. First, how does
374 radial and osmotic stretch lead to the activation of store-operated calcium signaling? Although Orai has not previously been shown to be mechanosensitive, our studies
376 revealed a requirement for Orai and its activator Stim in mechanically-evoked calcium flux in *Drosophila* epidermal cells. We also showed that radial stretch of human
378 keratinocytes triggered calcium release from stores and SOCE; our previous studies showed that Stim and Orai are required for SOCE in human keratinocytes (Wilson *et al.*,
380 2013). These data in combination with previous findings that showed mechanical stimulation of human mesenchymal stem cells also triggers SOCE (Kim *et al.*, 2015)
382 suggests that Stim/Orai signaling may represent a conserved pathway for mechanotransduction in non-neuronal cells.

384 Second, how is Stim/Orai function linked to mechanotransduction? Stim/Orai signaling is activated downstream of G-protein coupled receptors (GPCRs) and receptor
386 tyrosine kinases (RTKs) through phospholipase C. Studies have shown that a number GPCRs are mechanosensitive (Chachisvilis *et al.*, 2006; Grosmaitre *et al.*, 2007;
388 Mederos y Schnitzler *et al.*, 2008; Connelly *et al.*, 2015; Xu *et al.*, 2018), though this has not been studied in epidermal cells. Alternatively, plasma membrane deformation has
390 been shown to induce ER-plasma membrane junctions (Venturini *et al.*, 2020; Aoki *et al.*, 2021), where Stim and Orai clusters accumulate and interact to drive calcium influx
392 (Luik *et al.*, 2008).

Third, how does mechanically-induced singaling in epidermal cells lead to
394 modulation of SSNs? Our data support a model whereby epidermal cells and multiple classes of SSNs are functionally coupled. Epidermal stimulation modulates activity of
396 nociceptive C4da neurons, mechanosensory C3da and Cho neurons, and proprioceptive C1da neurons, and the output of neuronal activity is required for
398 epidermis-evoked behaviors. We demonstrated a requirement for dynamin-dependent vesicle release from epidermal cells in mechanical sensitization, providing a potential
400 link between Stim/Orai signaling in epidermal cells and downstream neuronal activity.

However, the mediators that are released by epidermal cells and the signaling
402 molecules in the nociceptors remain unknown. Furthermore, whether different subtypes
of SSNs are coupled to epidermal cells by distinct mechanisms remains to be
404 determined. At least in the case of Cho neurons which are wrapped by ensheathing glial
cells and scolopale cells, signaling from epidermal cells likely involves at least one
406 additional cell type.

Epidermal cells ensheath peripheral arbors of some SSNs, including *Drosophila*
408 nociceptive C4da neurons and, to a lesser extent, mechanosensory C3da neurons
(Jiang *et al.*, 2019). Hence, epidermal sheaths could facilitate transduction of epidermal
410 signals that modulate nociceptor function. Consistent with this possibility, blocking
ensheathment attenuates *Drosophila* larval responses to noxious mechanical stimuli
412 (Jiang *et al.*, 2019) and likewise impairs function of some *C. elegans* mechanosensory
neurons (Chen and Chalfie, 2014). However, our finding that epidermal stimulation
414 evokes calcium responses from SSNs that are not ensheathed by epidermal cells
(C1da, Cho neurons) argues that epidermal sheaths are unlikely to play an essential
416 function in epidermis-SSN functional copuling. Instead, ensheathment may facilitate
nociceptor activation by increasing the efficiency of vesicular exchange or, alternatively,
418 may modulate nociceptor activity through through enhanced ionic coupling to epidermal
cells.

420 Which epidermal-derived molecules might modulate neuronal activity? There are
several mechanisms by which mammalian epidermal cells activate SSNs. Vesicular
422 release of norepinephrine from mouse epidermal Merkel cells is required for sustained
touch-evoked firing of mechanosensory neurons (Hoffman *et al.*, 2018). Additionally,
424 mechanical stimuli trigger ATP release from mouse keratinocytes that activates
nociceptors via purinergic (P2X4) receptors (Koizumi *et al.*, 2004; Tsutsumi *et al.*, 2009;
426 Moehring *et al.*, 2018). Finally, Stim/Orai-dependent SOCE mediates the release of the
cytokine thymic stromal lymphopoietin (TSLP) from keratinocytes that directly activates
428 a subset of TRPA1-expressing SSNs to induce itch (Wilson *et al.*, 2013). Similar to
these mammalian models, UV-damage has been shown to induce the release of the
430 cytokine Eiger to promote nociceptor sensitization (Babcock *et al.*, 2009); though this

occurred on a slower timescale than the epidermal-evoked mechanical sensitization we
432 describe here (8 hrs vs. ~ 10 sec, Fig. 4L). Likewise, epidermal platelet-derived growth factor (PDGF) ligands regulate mechanonociceptive responses in *Drosophila* (Lopez-
434 Bellido *et al.*, 2019) and intrathecal delivery of PDGF or the closely related growth factor EGFR yields mechanical hypersensitivity in rats (Masuda *et al.*, 2009; Puig *et al.*, 2020),
436 but it remains to be determined whether growth factor signaling can yield rapid sensitization. Hence, future studies will address which neurotransmitters,
438 neuropeptides, or inflammatory mediators underly epidermal cell-mediated mechanical sensitization.

440 Our data support a model whereby epidermal cells and multiple classes of SSNs are functionally coupled. Future studies will address which neurotransmitters,
442 neuropeptides, or inflammatory mediators underly epidermal cell-mediated mechanical sensitization. An additional key next step is understanding whether the neuronal
444 plasticity underlying mechanical sensitization results from the direct modulation of mechanosensitive channels or rapid insertion of new mechanosensitive channels into
446 the plasma membrane, or from changes in the signaling pathways or channels that regulate neuronal excitability. Overall, we performed an unbiased genetic screen that for
448 the first time establishes a key role for mechanically-evoked Stim/Orai calcium signaling in epidermal cells that drive nociceptor modulation and mechanical hypersensitivity.
450

Material and Methods

452 ***Drosophila strains***

Flies were maintained on standard cornmeal-molasses-agar media and reared at 25° C
454 under 12 h alternating light-dark cycles. For all experiments involving optogenetic manipulations, larvae were raised in the constant dark at 25 °C on Nutri-Fly Instant
456 Food (Genesee Scientific #66-117), supplemented with 1 mM all-trans retinal (ATR; Sigma #R2500). See Table S1 for a complete list of alleles used in this study.
458 Experimental genotypes are listed in figure legends.

460 **Behavior analysis**

Optogenetic behavior screen

462 Individual larvae were rinsed in ddH2O, transferred to an agarose substrate (1% agarose, 100 mM dish) in a darkened arena, and habituated for 30 sec. Larvae were
464 stimulated with a top-mounted 488 nM LED illuminator (PE-300, CoolLED) and images were captured with a sCMOS camera (Orca Flash 3.0, Hamamatsu) at frame
466 acquisition rate of 20 fps and behaviors were scored before, during and after optogenetic stimulation.

468

High resolution video tracking of optogenetic-gated larval behavior

470 Following 5 min of light deprivation including 15 sec of habituation in the behavioral arena, larvae were tracked before, during and after optical stimulus (10 sec each, 30
472 sec total) (Fig. 2A). For these studies we modified our stimulation paradigm in two key ways: to avoid potential contributions of nociceptor light evoked responses (Xiang *et al.*,
474 2010), we stimulated larvae using yellow-shifted light; and to facilitate kinetic analysis of behavior outputs, we used an automated shutter. Larvae were stimulated with a top-
476 mounted 585 nm LED illuminator (SPECTRA X, Lumencor) equipped with a filter (FF01 585/40-25, Semrock), and images were captured with a sCMOS camera (Zyla4.2,
478 Andor) at a frame rate of 20Hz. Larvae were constantly illuminated with an infrared (940 nm) light source (LDR2-132IR2-940-LA, CSS) for visualization. Larvae were fed (ATR+)
480 or vehicle alone (ATR-) as indicated.

482 *Thermogenetic behavior assays*

Larvae for thermogenetic assays were reared at room temperature (20° C) to limit
484 TRPA1 activation during development. Third instar larvae were isolated from their food, washed in distilled water, and recovered to damp agar plates for several min, and
486 transferred individually to a Peltier plate held at 25° C or 35° C. Behavior responses were recorded under infrared light with a computer-controlled GigE camera (FLIR) at an
488 acquisition rate of 20 fps for 20 sec. Responses were analyzed post-hoc blind to genotype and were plotted as the proportion of larvae that exhibited at least one
490 complete nocifensive roll during stimulus application.

492 *Mechanonociception assays*

Third instar larvae were isolated from their food, washed in distilled water, and placed
494 on a scored 35 mm petri dish with a thin film of water such that larvae stayed moist but
did not float. Larvae were stimulated dorsally between segments A4 and A7 with
496 calibrated Von Frey filaments that delivered the indicated force upon buckling, and
nocifensive rolling responses were scored during the 10 sec following stimulus removal.
498 For assays involving multiple stimuli, larvae were stimulated individually, allowed to
freely locomote in the arena for up to 1 min (for longer recoveries larvae were recovered
500 onto 2% agar to prevent desiccation), and subsequently presented with the second
stimulus. For assays involving thermal and mechanical stimuli, larvae were individually
502 transferred to a pre-warmed Peltier plate containing a thin layer of water, incubated for
the indicated time, and transferred to the behavior arena (or a 2% agar plate for
504 recoveries > 1 min) with a paint brush for subsequent mechanical stimulation. All assays
were conducted in ambient light except for experiments with GtACR (Fig. S72), which
506 were conducted under broad-spectrum (500-700 nm) LED illumination (CoolLED PE-
300, green). Our illumination setup for these experiments provided limited working
508 distance, therefore larvae were restrained with forceps and given only a single stimulus.

510 *Video annotations*

Videos of individual larvae responding to light stimuli were scored on a frame-by-frame
512 basis using the annotation software BORIS (Friard and Gamba, 2016). Behaviors
scored, along with descriptions of the criteria for each behavior, are detailed in Table
514 S2. Video analysts were blind to the genotype and treatment during scoring. Scoring on
a training set was compared across all analysts to calibrate, and any behaviors for
516 which the primary analyst was uncertain were reviewed by an additional analyst.
Additionally, 10% of videos were scored independently by two analysts and there was at
518 least 80% concordance in behaviors annotated in these comparisons.

520 **Microscopy**

Calcium imaging: ventral nerve cords

522 Third-instar larvae were dissected along the dorsal midline and pinned on a sylgard-coated dish (Silpot 184, Dow Corning Toray). The internal organs except for neural
524 tissues were removed. Larvae were bathed in HL3.1 (Feng et al, 2004) modified to remove calcium (Table S3) to minimize larval movement. The ventral nerve cord was
526 imaged using an Olympus BX51WI microscope, equipped with a spinning-disk confocal unit Yokogawa CSU10 (Yokogawa) and an EM-CCD digital camera (Evolve,
528 Photometrics). For activation of epidermal cells with the light gated CsChrimson, red light was delivered by a pE-300 (CoolLED) equipped with a filter (ET645/30x, Chroma).
530 Obtained images were analyzed using Metamorph (https://www.moleculardevices.com/systems/metamorph-research-imaging) and ImageJ
532 (Schneider *et al.*, 2012). Baseline fluorescence was calculated as the mean fluorescence intensity of an ROI over the ten frames prior to light stimulus delivery. The
534 trapezoidal method was used to calculate area under the curve, utilizing the trapz function of MATLAB. Data points from the onset of stimulation to the end of stimulation
536 were used for the calculation.

538 *Calcium imaging: fillet preparations*

Third-instar larvae were dissected along the ventral midline and pinned on sylgard (Dow
540 Corning) dishes with the internal surface facing towards the microscope. All internal organs, including the central nervous system, were removed. Larvae were bathed in
542 calcium-containing HL3.1 (Feng *et al.*, 2004) (Table S3) except where indicated and images of the dorsal midline between abdominal segments A2 and A4 were captured
544 with a Zeiss Axio Zoom V16 microscope. Captured images were analyzed using ImageJ (Schneider *et al.*, 2012). Mechanical stimulus: fillets were poked with a tapered
546 borosilicate capillary with a rounded tip, using a micromanipulator to induce a deflection of 25 μm. The decay time constant was calculated by fitting the data points from the
548 peak response to the end of the experiment into an exponential curve $f(x) = a*\exp(b*x)$ using MATLAB with $R^2>0.9$ used as a threshold for reliable fitting.

550

Calcium imaging: dissociated epidermal cells

552 Six to eight larval fillets were dissociated in 400 μL of 50% Saline (modified Ringer's
recipe) / 50% Schneider's media with 200 U/mL collagenase type I (Fisher 17-100-017),
554 with mixing at 1000 RPM at 33°C for 16 min, with trituration every 8 min. Undigested
fillets were removed and the remaining suspension was spun at 500 g for 3 min,
556 followed by aspiration of the supernatant down to a 10 μL cell suspension. Cells were
resuspended in 30 μL fresh PBS / Schneider's solution and plated onto poly-D-lysine (1
558 mg/ml, Sigma P7886) coated No. 1 coverslips, with 10 μL cell solution per coverslip.
Cells were cultured at least 30 min and up to 2 hr at 25° C prior to imaging. Cells were
560 imaged using a a 10x objective at a frame rate of 0.33 Hz. Solutions are indicated in
figure legends (see Table S3 for recipes). Obtained images were analyzed using
562 MetaFluor and Python and baseline fluorescence was calculated as the mean
fluorescence intensity of an ROI over 5 frames prior to stimulus delivery. For stretch
564 stimulation, circular membranes were cut with an arch punch from sheets of glossy
silicone of 0.01–0.02 inch thickness (Specialty Manufacturing, Inc.) and coated with 1
566 mg/ml poly-D-lysine for 1 h before plating cells. Membranes were mounted onto the
StageFlexer system and vacuum pressure was applied through the FX-3000 system
568 (Flexcell). Calibrations were performed using fluorescent beads attached to the
membranes, and images were taken before and during a static stretch. To stimulate
570 cells, a 2 sec square wave of vacuum pressure was applied. Cells were imaged with an
Olympus BX61WI upright microscope. For store-operated calcium entry measurements
572 and osmotic stimulation, cells were imaged using a Zeiss Observer inverted microscope
and solutions were perfused using the Automate Scientific ValveLink 8.2 perfusion
574 system. At the end of each imaging session, 1uM ionomycin was perfused and only
cells that showed a calcium response, as defined by a 10% increase from baseline
576 fluorescence, were used in analysis. Flow, osmotic and radial stretch responders were
defined by a 5% increase from baseline fluorescence.
578

Calcium imaging: human keratinocytes

580 Immortalized human keratinocytes (HaCaT) cells were plated on silicone membranes one day prior to stretch experiments. Prior to the radial stretch experiments, cells were
582 loaded with 1 µm Fura-2AM supplemented with 0.01% Pluronic F-127 (w/v, Life Technologies) in a physiological Ringer's solution containing the following (in mm): 140
584 NaCl, 5 KCl, 10 HEPES, 2 CaCl2, 2 MgCl2, and 10 d-(+)-glucose, pH 7.4. Acquired images were displayed as the ratio of 340 nm/380 nm. Cells that had a response 10
586 standard deviations above baseline to ionomycin were included in the analysis and stretch responses were defined by a 15% increase in Fura-2 340/380 ratio.
588

Confocal Microscopy

590 For peripheral imaging of cellular morphology, live single larvae were mounted in 90% glycerol under a coverslip and imaged on a Leica SP5 confocal microscope using a 40x
592 1.25 NA lens. To image the larval CNS, larvae were dissected on sylgard plates, briefly fixed in 4% paraformaldehyde (PFA) in PBS for 15 min at room temperature, washed 3
594 x 5 min in PBS, and mounted for imaging.

596 **RNA-Seq analysis of epidermal cells**

RNA isolation for RNA-Seq

598 Larvae with cytoplasmic GFP expressed in different epidermal subsets were microdissected and dissociated in collagenase type I (Fisher 17-100-017) into single cell
600 suspensions, largely as previously described (Williams *et al.*, 2016), with the addition of 1% BSA to the dissociation mix. After dissociation, cells were transferred to a new 35
602 mm petri dish with 1 mL 50% Schneider's media, 50% PBS supplemented with 1% BSA. Under a fluorescent stereoscope, individual fluorescent cells were manually
604 aspirated with a glass pipette into PBS with 0.5% BSA, and then serially transferred until isolated without any additional cellular debris present. Ten cells per sample were
606 aspirated together, transferred to a mini-well containing 3ul lysis solution (0.2 % Triton X-100 in water with 2 U / µL RNAse Inhibitor), lysed by pipetting up and down several
608 times, transferred to a microtube, and stored at -80° C. For the picked cells, 2.3 µL of lysis solution was used as input for library preparation.

610

RNA-Seq library preparation

612 RNA-Seq libraries were prepared from the picked cells following the Smart-Seq2 protocol for full length transcriptomes (Picelli *et al.*, 2014). To minimize batch effects,
614 primers, enzymes, and buffers were all used from the same lots for all libraries. Libraries were multiplexed, pooled, and purified using AMPure XP beads, quality was
616 checked on an Agilent TapeStation, and libraries were sequenced as 51-bp single end reads on a HiSeq4000 at the UCSF Center for Advanced Technology.

618

RNA-Seq data analysis

620 Reads were demultiplexed with CASAVA (Illumina) and read quality was assessed using FastQC (https://www.bioinformatics.babraham.ac.uk/) and MultiQC (Ewels *et al.*,
622 2016). Reads containing adapters were removed using Cutadapt version 2.4 (Martin, 2011) and reads were mapped to the *D. melanogaster* transcriptome, FlyBase genome
624 release 6.29, using Kallisto version 0.46.0 (Bray *et al.*, 2016) with default parameters. AA samples were removed from further analysis for poor quality, including low read
626 depth (< 500,000 reads), and low mapping rates (< 80%). Raw sequencing reads and gene expression estimates are available in the NCBI Sequence Read Archive (SRA)
628 and in the Gene Expression Omnibus (GEO) under accession number SUB11489996.

630 **Statistical analysis**

For each experimental assay control populations were sampled to estimate appropriate
632 sample numbers to allow detection of ~33% differences in means with 80% power over a 95% confidence interval. Details of statistical tests including treatment groups, sample
634 numbers, statistical tests, p-values and q-values are provided in the experimental supplement.

636

Acknowledgements

638 This work was supported by grants from the National Institutes of Health to J.Z.P. (NINDS R01 NS076614), DB (NICHD K99 HD086271), CW (5F31NS106775), and the

640 MBL (R25NS063307); a grant from the National Science Foundation to S.S.M (NSF GRFP DGE1752814); a grant from the Weill Neurohub to J.Z.P and D.B.; a grant from
642 the Scan Design Foundation, a JSPS long-term fellowship and startup funds from UW (J.Z.P); MEXT Grants-in-Aid for Scientific Research (KAKENHI 16H06456), JSPS
644 (KAKENHI 16H02504), WPI-IRCN, AMED-CREST (JP22gm310010), and JST-CREST to KE; and a fellowship from the Grass Foundation (C.E.E.). Fly Stocks obtained from
646 the Bloomington *Drosophila* Stock Center (NIH P40OD018537) were used in this study. We thank Jessica Huang, Jordan Martel, and David Shen for assistance with video
648 tracking; Peter Soba for helpful discussions.

650 **Author Contributions**

Conception and design: Optogenetic behavior analysis, K.E., J.Z.P, C.R.W, J.Y.; larval
652 behavior assays, J.Z.P, C.R.W, and J.Y.; in vivo calcium imaging, K.E., J.Z.P, C.R.W, J.Y.; ex vivo calcium imaging, D.B., S.S.M., and J.Z.P
654 *Acquisition of data*: Optogenetic behavior screen, C.J.A, C.E.E., S.M., and J.Y.; Optogenetic behavior assays, J.Y., C.H., M.M., K.I., and C.R.W.; mechanonociception
656 assays, C.R.W, and J.Z.P; thermogenetic behavior assays, J.Z.P.; RNA-sequencing, J.Z.P. and C.R.W.
658 *Analysis and Interpretation of data*: larval behavior assays, J.Z.P, C.R.W, J.Y.; in vivo calcium imaging, K.E., J.Z.P, C.R.W, J.Y.; ex vivo calcium imaging, D.B. and S.S.M.;
660 transcriptomic data, C.H., C.R.W., and J.Z.P.
Drafting the article: D.B., J.Z.P, C.R.W, S.S.M., and J.Y.

662

Competing Interests

664 DMB is on the scientific advisory board of Escient Pharmaceuticals. The remaining authors declare no conflicts of interest.

666

References

668 Aoki, K, Harada, S, Kawaji, K, Matsuzawa, K, Uchida, S, and Ikenouchi, J (2021). STIM-Orai1 signaling regulates fluidity of cytoplasm during membrane blebbing. Nat Commun 12, 480.

670 Ashmole, I, Duffy, SM, Leyland, ML, Morrison, VS, Begg, M, and Bradding, P (2012). CRACM/Orai ion channel expression and function in human lung mast cells. J Allergy Clin Immunol 129, 1628-
672 1635.e2.

Babcock, DT, Landry, C, and Galko, MJ (2009). Cytokine signaling mediates UV-induced
674 nociceptive sensitization in Drosophila larvae. Curr Biol 19, 799–806.

Bautista, DM, Jordt, S-E, Nikai, T, Tsuruda, PR, Read, AJ, Poblete, J, Yamoah, EN, Basbaum, AI,
676 and Julius, D (2006). TRPA1 mediates the inflammatory actions of environmental irritants and proalgesic agents. Cell 124, 1269–1282.

678 Boiko, N et al. (2017). TrpA1 activation in peripheral sensory neurons underlies the ionic basis of pain hypersensitivity in response to vinca alkaloids. PLoS ONE 12, e0186888.

680 Bray, NL, Pimentel, H, Melsted, P, and Pachter, L (2016). Near-optimal probabilistic RNA-seq quantification. Nat Biotechnol 34, 525–527.

682 Burgos, A et al. (2018). Nociceptive interneurons control modular motor pathways to promote escape behavior in Drosophila. Elife 7.

684 Cauna, N (1973). The free penicillate nerve endings of the human hairy skin. J Anat 115, 277–288.

686 Chachisvilis, M, Zhang, Y-L, and Frangos, JA (2006). G protein-coupled receptors sense fluid shear stress in endothelial cells. Proc Natl Acad Sci U S A 103, 15463–15468.

688 Chalfie, M, and Sulston, J (1981). Developmental genetics of the mechanosensory neurons of Caenorhabditis elegans. Dev Biol 82, 358–370.

690 Chanaday, NL, Nosyreva, E, Shin, O-H, Zhang, H, Aklan, I, Atasoy, D, Bezprozvanny, I, and Kavalali, ET (2021). Presynaptic store-operated Ca2+ entry drives excitatory spontaneous
692 neurotransmission and augments endoplasmic reticulum stress. Neuron 109, 1314-1332.e5.

Chen, X, and Chalfie, M (2014). Modulation of C. elegans touch sensitivity is integrated at
694 multiple levels. J Neurosci 34, 6522–6536.

Chung, M-K, Lee, H, Mizuno, A, Suzuki, M, and Caterina, MJ (2004). TRPV3 and TRPV4 mediate
696 warmth-evoked currents in primary mouse keratinocytes. J Biol Chem 279, 21569–21575.

Connelly, T, Yu, Y, Grosmaitre, X, Wang, J, Santarelli, LC, Savigner, A, Qiao, X, Wang, Z, Storm,
698 DR, and Ma, M (2015). G protein-coupled odorant receptors underlie mechanosensitivity in mammalian olfactory sensory neurons. Proc Natl Acad Sci U S A 112, 590–595.

700 Ewels, P, Magnusson, M, Lundin, S, and Käller, M (2016). MultiQC: summarize analysis results for multiple tools and samples in a single report. Bioinformatics 32, 3047–3048.

702 Feng, Y, Ueda, A, and Wu, C-F (2004). A modified minimal hemolymph-like solution, HL3.1, for physiological recordings at the neuromuscular junctions of normal and mutant Drosophila
704 larvae. J Neurogenet 18, 377–402.

Feske, S, Gwack, Y, Prakriya, M, Srikanth, S, Puppel, S-H, Tanasa, B, Hogan, PG, Lewis, RS, Daly,
706 M, and Rao, A (2006). A mutation in Orai1 causes immune deficiency by abrogating CRAC channel function. Nature 441, 179–185.

708 Fink, M, Duprat, F, Lesage, F, Reyes, R, Romey, G, Heurteaux, C, and Lazdunski, M (1996). Cloning, functional expression and brain localization of a novel unconventional outward
710 rectifier K+ channel. EMBO J 15, 6854–6862.

Friard, O, and Gamba, M (2016). BORIS: a free, versatile open-source event-logging software for
712 video/audio coding and live observations. Methods in Ecology and Evolution 7, 1325–1330.

Galko, MJ, and Krasnow, MA (2004). Cellular and genetic analysis of wound healing in
714 Drosophila larvae. PLoS Biol 2, E239.

Gorczyca, DA, Younger, S, Meltzer, S, Kim, SE, Cheng, L, Song, W, Lee, HY, Jan, LY, and Jan, YN
716 (2014). Identification of Ppk26, a DEG/ENaC Channel Functioning with Ppk1 in a Mutually Dependent Manner to Guide Locomotion Behavior in Drosophila. Cell Rep 9, 1446–1458.

718 Grosmaitre, X, Santarelli, LC, Tan, J, Luo, M, and Ma, M (2007). Dual functions of mammalian olfactory sensory neurons as odor detectors and mechanical sensors. Nat Neurosci 10, 348–
720 354.

Guo, Y, Wang, Y, Wang, Q, and Wang, Z (2014). The role of PPK26 in Drosophila larval
722 mechanical nociception. Cell Rep 9, 1183–1190.

Haeberle, H, Bryan, LA, Vadakkan, TJ, Dickinson, ME, and Lumpkin, EA (2008). Swelling-
724 activated Ca2+ channels trigger Ca2+ signals in Merkel cells. PLoS One 3, e1750.

Hamada, FN, Rosenzweig, M, Kang, K, Pulver, SR, Ghezzi, A, Jegla, TJ, and Garrity, PA (2008). An
726 internal thermal sensor controlling temperature preference in Drosophila. Nature 454, 217–220.

728 Han, C, Wang, D, Soba, P, Zhu, S, Lin, X, Jan, LY, and Jan, Y-N (2012). Integrins regulate repulsion-mediated dendritic patterning of drosophila sensory neurons by restricting dendrites
730 in a 2D space. Neuron 73, 64–78.

Hoffman, BU, Baba, Y, Griffith, TN, Mosharov, EV, Woo, S-H, Roybal, DD, Karsenty, G,
732 Patapoutian, A, Sulzer, D, and Lumpkin, EA (2018). Merkel Cells Activate Sensory Neural Pathways through Adrenergic Synapses. Neuron 100, 1401-1413.e6.

734 Hoover, PJ, and Lewis, RS (2011). Stoichiometric requirements for trapping and gating of Ca2+ release-activated Ca2+ (CRAC) channels by stromal interaction molecule 1 (STIM1). Proc Natl
736 Acad Sci U S A 108, 13299–13304.

Hu, C et al. (2017). Sensory integration and neuromodulatory feedback facilitate Drosophila
738 mechanonociceptive behavior. Nat Neurosci 20, 1085–1095.

Hwang, RY, Zhong, L, Xu, Y, Johnson, T, Zhang, F, Deisseroth, K, and Tracey, WD (2007).
740 Nociceptive neurons protect Drosophila larvae from parasitoid wasps. Curr Biol 17, 2105–2116.

Jiang, N et al. (2019). A conserved morphogenetic mechanism for epidermal ensheathment of
742 nociceptive sensory neurites. Elife 8.

Jiang, N, Soba, P, Parker, E, Kim, CC, and Parrish, JZ (2014). The microRNA bantam regulates a
744 developmental transition in epithelial cells that restricts sensory dendrite growth. Development 141, 2657–2668.

746 Khuong, TM, Wang, Q-P, Manion, J, Oyston, LJ, Lau, M-T, Towler, H, Lin, YQ, and Neely, GG (2019). Nerve injury drives a heightened state of vigilance and neuropathic sensitization in
748 Drosophila. Sci Adv 5, eaaw4099.

Kim, ME, Shrestha, BR, Blazeski, R, Mason, CA, and Grueber, WB (2012a). Integrins establish
750 dendrite-substrate relationships that promote dendritic self-avoidance and patterning in drosophila sensory neurons. Neuron 73, 79–91.

752 Kim, SE, Coste, B, Chadha, A, Cook, B, and Patapoutian, A (2012b). The role of Drosophila Piezo in mechanical nociception. Nature 483, 209–212.

754 Kim, T-J et al. (2015). Distinct mechanisms regulating mechanical force-induced Ca^{2+} signals at the plasma membrane and the ER in human MSCs. Elife 4, e04876.

756 Klapoetke, NC et al. (2014). Independent optical excitation of distinct neural populations. Nature Methods 11, 338–346.

758 Koenig, JH, Saito, K, and Ikeda, K (1983). Reversible control of synaptic transmission in a single gene mutant of Drosophila melanogaster. J Cell Biol 96, 1517–1522.

760 Koizumi, S, Fujishita, K, Inoue, K, Shigemoto-Mogami, Y, Tsuda, M, and Inoue, K (2004). Ca2+ waves in keratinocytes are transmitted to sensory neurons: the involvement of extracellular
762 ATP and P2Y2 receptor activation. Biochem J 380, 329–338.

Liu, X, Wang, H, Jiang, Y, Zheng, Q, Petrus, M, Zhang, M, Zheng, S, Schmedt, C, Dong, X, and
764 Xiao, B (2019). STIM1 thermosensitivity defines the optimal preference temperature for warm sensation in mice. Cell Res 29, 95–109.

766 Lopez-Bellido, R, Puig, S, Huang, PJ, Tsai, C-R, Turner, HN, Galko, MJ, and Gutstein, HB (2019).
Growth Factor Signaling Regulates Mechanical Nociception in Flies and Vertebrates. J Neurosci
768 39, 6012–6030.

Luik, RM, Wang, B, Prakriya, M, Wu, MM, and Lewis, RS (2008). Oligomerization of STIM1
770 couples ER calcium depletion to CRAC channel activation. Nature 454, 538–542.

Maksimovic, S et al. (2014). Epidermal Merkel cells are mechanosensory cells that tune
772 mammalian touch receptors. Nature 509, 617–621.

Mandadi, S, Sokabe, T, Shibasaki, K, Katanosaka, K, Mizuno, A, Moqrich, A, Patapoutian, A,
774 Fukumi-Tominaga, T, Mizumura, K, and Tominaga, M (2009). TRPV3 in keratinocytes transmits
temperature information to sensory neurons via ATP. Pflugers Arch 458, 1093–1102.

776 Maneshi, MM et al. (2020). Orai1 Channels Are Essential for Amplification of Glutamate-Evoked
Ca2+ Signals in Dendritic Spines to Regulate Working and Associative Memory. Cell Rep 33,
778 108464.

Masuda, J, Tsuda, M, Tozaki-Saitoh, H, and Inoue, K (2009). Intrathecal delivery of PDGF
780 produces tactile allodynia through its receptors in spinal microglia. Mol Pain 5, 23.

Mauthner, SE, Hwang, RY, Lewis, AH, Xiao, Q, Tsubouchi, A, Wang, Y, Honjo, K, Skene, JHP,
782 Grandl, J, and Tracey, WD (2014). Balboa binds to pickpocket in vivo and is required for
mechanical nociception in Drosophila larvae. Curr Biol 24, 2920–2925.

784 Mederos y Schnitzler, M, Storch, U, Meibers, S, Nurwakagari, P, Breit, A, Essin, K, Gollasch, M,
and Gudermann, T (2008). Gq-coupled receptors as mechanosensors mediating myogenic
786 vasoconstriction. EMBO J 27, 3092–3103.

Moehring, F, Cowie, AM, Menzel, AD, Weyer, AD, Grzybowski, M, Arzua, T, Geurts, AM, Palygin,
788 O, and Stucky, CL (2018). Keratinocytes mediate innocuous and noxious touch via ATP-P2X4
signaling. Elife 7.

790 Mohammad, F, Stewart, JC, Ott, S, Chlebikova, K, Chua, JY, Koh, T-W, Ho, J, and Claridge-Chang,
A (2017). Optogenetic inhibition of behavior with anion channelrhodopsins. Nat Methods 14,
792 271–274.

Moqrich, A, Hwang, SW, Earley, TJ, Petrus, MJ, Murray, AN, Spencer, KSR, Andahazy, M, Story,
794 GM, and Patapoutian, A (2005). Impaired thermosensation in mice lacking TRPV3, a heat and
camphor sensor in the skin. Science 307, 1468–1472.

796 Morin, X, Daneman, R, Zavortink, M, and Chia, W (2001). A protein trap strategy to detect GFP-
tagged proteins expressed from their endogenous loci in Drosophila. Proc Natl Acad Sci USA 98,
798 15050–15055.

O'Brien, GS, Rieger, S, Wang, F, Smolen, GA, Gonzalez, RE, Buchanan, J, and Sagasti, A (2012).
800 Coordinate development of skin cells and cutaneous sensory axons in zebrafish. J Comp Neurol 520, 816–831.

802 Ohyama, T et al. (2015). A multilevel multimodal circuit enhances action selection in Drosophila. Nature 520, 633–639.

804 Picelli, S, Faridani, OR, Björklund, AK, Winberg, G, Sagasser, S, and Sandberg, R (2014). Full-length RNA-seq from single cells using Smart-seq2. Nat Protoc 9, 171–181.

806 Pores-Fernando, AT, and Zweifach, A (2009). Calcium influx and signaling in cytotoxic T-lymphocyte lytic granule exocytosis. Immunol Rev 231, 160–173.

808 Puig, S, Donica, CL, and Gutstein, HB (2020). EGFR Signaling Causes Morphine Tolerance and Mechanical Sensitization in Rats. ENeuro 7, ENEURO.0460-18.2020.

810 Ramesh, G et al. (2021). A short isoform of STIM1 confers frequency-dependent synaptic enhancement. Cell Rep 34, 108844.

812 Ranade, SS et al. (2014). Piezo2 is the major transducer of mechanical forces for touch sensation in mice. Nature 516, 121–125.

814 Robertson, JL, Tsubouchi, A, and Tracey, WD (2013). Larval defense against attack from parasitoid wasps requires nociceptive neurons. PLoS One 8, e78704.

816 Sadler, KE, Moehring, F, and Stucky, CL (2020). Keratinocytes contribute to normal cold and heat sensation. Elife 9, e58625.

818 Schneider, CA, Rasband, WS, and Eliceiri, KW (2012). NIH Image to ImageJ: 25 years of image analysis. Nat Methods 9, 671–675.

820 Sweeney, ST, Broadie, K, Keane, J, Niemann, H, and O'Kane, CJ (1995). Targeted expression of tetanus toxin light chain in Drosophila specifically eliminates synaptic transmission and causes
822 behavioral defects. Neuron 14, 341–351.

Tsutsumi, M, Inoue, K, Denda, S, Ikeyama, K, Goto, M, and Denda, M (2009). Mechanical-
824 stimulation-evoked calcium waves in proliferating and differentiated human keratinocytes. Cell Tissue Res 338, 99–106.

826 Turner, HN et al. (2016). The TRP Channels Pkd2, NompC, and Trpm Act in Cold-Sensing Neurons to Mediate Unique Aversive Behaviors to Noxious Cold in Drosophila. Curr Biol 26,
828 3116–3128.

Venturini, V et al. (2020). The nucleus measures shape changes for cellular proprioception to
830 control dynamic cell behavior. Science 370, eaba2644.

Williams, CR, Baccarella, A, Parrish, JZ, and Kim, CC (2016). Trimming of sequence reads alters
832 RNA-Seq gene expression estimates. BMC Bioinformatics 17, 103.

Wilson, SR, Thé, L, Batia, LM, Beattie, K, Katibah, GE, McClain, SP, Pellegrino, M, Estandian, DM,
834 and Bautista, DM (2013). The epithelial cell-derived atopic dermatitis cytokine TSLP activates neurons to induce itch. Cell 155, 285–295.

836 Woo, S-H et al. (2014). Piezo2 is required for Merkel-cell mechanotransduction. Nature 509, 622–626.

838 Xiang, Y, Yuan, Q, Vogt, N, Looger, LL, Jan, LY, and Jan, YN (2010). Light-avoidance-mediating photoreceptors tile the Drosophila larval body wall. Nature 468, 921–926.

840 Xu, J et al. (2018). GPR68 Senses Flow and Is Essential for Vascular Physiology. Cell 173, 762-775.e16.

842 Yamamoto, M, Ueda, R, Takahashi, K, Saigo, K, and Uemura, T (2006). Control of axonal sprouting and dendrite branching by the Nrg-Ank complex at the neuron-glia interface. Curr Biol
844 16, 1678–1683.

Yin, C, Peterman, E, Rasmussen, JP, and Parrish, JZ (2021). Transparent Touch: Insights From
846 Model Systems on Epidermal Control of Somatosensory Innervation. Front Cell Neurosci 15, 680345.

848 Zhang, W, Yan, Z, Jan, LY, and Jan, YN (2013). Sound response mediated by the TRP channels NOMPC, NANCHUNG, and INACTIVE in chordotonal organs of Drosophila larvae. Proc Natl Acad
850 Sci USA 110, 13612–13617.

Zhong, L, Hwang, RY, and Tracey, WD (2010). Pickpocket is a DEG/ENaC protein required for
852 mechanical nociception in Drosophila larvae. Curr Biol 20, 429–434.

Zimmermann, G, Wang, L-P, Vaughan, AG, Manoli, DS, Zhang, F, Deisseroth, K, Baker, BS, and
854 Scott, MP (2009). Manipulation of an innate escape response in Drosophila: photoexcitation of acj6 neurons induces the escape response. PLoS One 4, e5100.

856

858 **Figure Legends**

860 **Figure 1. Stimulation of epidermal cells elicits nociceptive behaviors.** (A) Fraction of larvae that exhibited optogenetic-induced rolling (roll probability) using the indicated
862 GAL4 lines to drive *UAS-CsChrimson* expression. All experimental genotypes, except for larvae expressing *UAS-CsChrimson* in C4da neurons, included *elav-GAL80* to
864 suppress neuronal GAL4 activity. Genotypes: *GAL4, UAS-CsChrimson, elav-GAL80/+*. (B) Roll probability of larvae following optogenetic stimulation using the indicated GAL4
866 lines in combination with *elav-GAL80* (or *tsh-GAL80* + *cha-GAL80* in the case of *A58-GAL4*) to drive *UAS-CsChrimson* expression in epidermal cells. All epidermal drivers
868 except for *sr-GAL4*, which is expressed in apodemes but no other epidermal cells, elicited rolling responses. Genotypes: *GAL4, UAS-CsChrimson, elav-GAL80/+*. (C) Roll
870 probability of larvae following thermogenetic stimulation using the indicated GAL4 line to express the warmth (35°C) -activated *UAS-TrpA1*. The number of rolling larvae (out of
872 50) is indicated for each group. Genotypes: *GAL4, UAS-TrpA1, GAL80 (as indicated)/+*. Control, *UAS-TrpA1/+*. Sample sizes are indicated in each panel. Asterisk (*) indicates
874 $p<0.05$ in this and subsequent figures. Details of statistical analyses, including tests performed, p-values, and q-values are provided in the supplemental materials..

876

Figure 1 – figure supplement 1. Related to Figure 1A. Detailed behavior analyses of
878 larvae following optogenetic stimulation using the indicated GAL4 lines to express *UAS-CsChrimson*. (A-G) Behavior ethograms show behaviors of individual larvae (rows) prior
880 to, during, and after application of the light stimulus (indicated by the blue bar above the ethogram). (H) Fraction of larvae exhibiting indicated behaviors and (I) duration of
882 indicated behaviors during light stimulus.

884 **Figure 1 – figure supplement 2**. Related to Figure 1A. Efficacy of *GAL80* transgenes. Maximum intensity projections show body wall expression patterns of (A) the pan-da
886 neuron driver $GAL4^{21-7}$ and (B) the nociceptor-specific driver *ppk-GAL4* with or without *elav-GAL80* to silence neuronal GAL4 expression. Note that *elav-GAL80* completely

888 suppresses GFP reporter expression from each of the drivers. Genotypes: (A) *GAL4*$^{21-7}$ *UAS-CD4-tdGFP/+* and *GAL4*$^{21-7}$ *UAS-CD4-tdGFP/+, elav-GAL-80/+*, (B) *ppk-GAL4,*
890 *UAS-CD4-tdGFP/+* and *ppk-GAL4, UAS-CD4-tdGFP/+, elav-GAL-80/+*.

892 **Figure 1 – figure supplement 3**. Related to Figures 1A and 1C. Expression patterns of body wall *GAL4* drivers. Maximum intensity projections of tiled confocal stacks show
894 larval expression of membrane-targeted RFP (*UAS-mCD2-Cherry*) by the indicated drivers in larvae additionally expressing the C4da neuron-specific marker *ppk-CD8-*
896 *GFP*. Scale bars, 500 μm. Genotypes: *ppk-mCD8-GFP/+; UAS-mCD2-Cherry/+; GAL4/+.*
898

900 **Figure 1 – figure supplement 4**. Related to Figure 1A. Epidermal manipulations have no effect on C4da neuron dendrte morphogeness. (A) Maximum intensity projections
902 show dendrites of representative C4da neurons labeled with *ppk-CD4-tdGFP* in the indicated treatment groups. (B) Morphometric analysis of C4da dendrites. Box plots
904 depict the total dendrite length (left) and the number of dendrite branchpoints (right) normalized to larval segmental area in larvae containing the pan-epidermal driver
906 *R38F11-GAL4* and the indicated *UAS*-transgenes at 120 h AEL. Prior to imaging, *ppk-CD4-tdGFP/+, R38F11-GAL4/UAS-shi*^{TS} larvae were incubated for 10 min at 30° C, as
908 in Fig. 6N. N $\geq$ 6 neurons for each genotype, points represent measurements from individual neurons, boxes display the first and third quartiles, hatches mark medians,
910 and whiskers mark maximum and minimum values. ANOVA with post-hoc Tukey's test revealed no significant difference between control and treatment groups for both
912 metrics. Genotypes: *ppk-CD4-tdGFP/+; R38F11-GAL4/+* without (-) or with a single copy of the indicated *UAS*-transgenes.
914

Figure 1 – figure supplement 5. Related to Figures 1A and 1C. Expression analysis of
916 the pan-epidermal *R38F11-GAL4* driver. (A-B) Maximum intensity projections of confocal stacks show larval expression of a red fluorescent protein (*UAS-tdTomato*)

918 under control of *R38F11-GAL4* in larvae additionally expressing *Nrg167-GFP*, an exon trap line that labels epidermal and glial membranes (Morin *et al.*, 2001; Yamamoto *et*
920 *al.*, 2006). (A) Low-magnification view showing stereotyped expression in dorsal epidermis across multiple larval segments. Larvae are oriented dorsal-up. *R38F11-*
922 *GAL4* is likewise expressed throughout the ventral and lateral epidermis. Compared to other epidermal drivers (see Fig. 1S5), *R38F11-GAL4* exhibited more uniform
924 expression from segment to segment and among epidermal subpopulations within a given segment. (B) *R38F11-GAL4* expression in the dorsal epidermis of a single
926 abdominal segment, A2. (C) High-resolution images of *R38F11-GAL4* expression visualized using a nuclear localized red fluorescent protein (*UAS-NLS-RFP*). Images
928 depict expression in larval skin territory containing dorsal cluster of SSNs (visualized by HRP immunoreactivity), which includes the nociceptive neuron ddaC (outlined by
930 dashed lines). Note that although *R38F11-GAL4* is expressed in epidermal cells, expression is undetectable in da neurons. The *R38F11-GAL4* expression domain
932 likewise excludes SSNs throughout the body wall. (D) *R38F11-GAL4* expression of *UAS-NLS-RFP* in the larval CNS. *R38F11-GAL4* is expressed in a single motor neuron
934 in each segment of the ventral ganglion, ~10 VNC interneurons, and <50 additional neurons in each brain hemisphere. (E-H) GAL80-mediated refinement of *R38F11-GAL4*
936 expression. (E) *Tsh-GAL80* induced variegation in epidermal *R38F11-GAL4* expression and (F) suppressed VNC expression while expanding brain expression domains of
938 *R38F11-GAL4*. (G) *Elav-GAL80* likewise induced epidermal variegation in *R38F11-GAL4* expression but (H) completely attenuated CNS expression. Dashed lines in (D, G,
940 and H) outline the larval brain and ventral ganglion. Genotypes: (A-B) *Nrg^{G00305}/+; UAS-tdTomato/+; GAL4^{GMR38F11}/+*, (C) *GAL4^{GMR38F11}/+, UAS-NLS-RedStinger/+*, (E-F)
942 *Nrg^{G00305}/+; UAS-tdTomato/tsh-GAL80; GAL4^{GMR38F11}/+*, (G-H) *Nrg^{G00305}/+; UAS-NLS-RedStinger/+; GAL4^{GMR38F11}/elav-GAL80*.

944

Figure 1 – figure supplement 6. Related to Figure 1B.

946 (A-B) Behaivior ethograms of larvae following pan-epidermal stimulation (denoted with a red bar) mediated by *A58-GAL4*. (C) Fraction of larvae exhibiting indicated behaviors

948 and (I) duration of indicated behaviors during optogenetic stimulation. (Genotype: *A58-GAL4, UAS-CsChrimson, tsh-GAL80, cha-GAL80/+*). (E-K) Behavioral ethograms of
950 larvae following optogenetic stimulation (denoted with a blue bar) with a panel of epidermal GAL4 drivers. (L) Fraction of larvae exhibiting indicated behaviors and (M)
952 duration of indicated behaviors during light stimulus. Genotype: *GAL4, UAS-CsChrimson, elav-GAL80/+*.

954

Figure 1 – figure supplement 7. Related to Figure 1B. Expression patterns of
956 epidermal GAL4 drivers in the larval body wall and CNS. (A) Maximum intensity projections of confocal stacks show larval expression of a red fluorescent protein (*UAS-*
958 *tdTomato*) under control of the indicated epidermal drivers in larvae additionally expressing *Nrg167-GFP*, an exon trap line that labels epidermal and glial membranes
960 (Morin *et al.*, 2001; Yamamoto *et al.*, 2006). White brackets mark the location of the dorsal cluster of SSNs, which are visualized at high resolution in (B). (B) Maximum
962 intensity projections of confocal stacks show larval expression of a nuclear-localized form of RFP (*UAS-RedStinger*) under control of the indicated *GAL4* drivers in larval
964 fillets stained with fluorescently conjugated anti-HRP antibody to label sensory neurons. The nociceptive C4da neuron soma is outlined with a white hatched line in composite
966 images and the outline is superimposed on images depicting *UAS-RedStinger* signal. Sensory neuron expression is undetectable for all epidermal drivers except for *A58-*
968 *GAL4*, for which stochhastic sensory neuron expression has been previously described (Jiang *et al.*, 2014). (C) Maximum intensity projections show CNS expression epidermal
970 drivers used in this study. Aside from *A58-GAL4*, each driver exhibits sparse nervous system expression. Genotypes: (A) Nrg^{G00305}*/+; UAS-tdTomato/+; GAL4/+*, (B-C) *UAS-*
972 *NLS-RFP/+; GAL4/+*.

974 **Figure 2.** Stimulation of epidermal cells evokes multimodal behavioral responses. (A) Larval behaviors were scored for 10 sec before, during, and after optogenetic
976 stimulation. (B-E) Fraction of larvae exhibiting indicated behaviors over time in one second bins expressing CsChrimson in (B) epidermal cells, (C) C4da neurons, (D) C3da

978 neurons, and (E) Cho neurons in the presence and absence of all-trans retinal (ATR).
Red line indicates the presence of light stimulation. (F) The latency to the first roll of the
980 larvae that rolled from *Epi>Chrimson* ATR+ and *C4da>Chrimson* ATR+ treatment
groups (n = 14, 17, respectively). (G) The duration of indicated behaviors of the larvae
982 that displayed those behaviors during optogenetic stimulation. (H) The fraction of larvae
that exhibited indicated behaviors following removal of the light stimulus of all larvae
984 from panels (B-E). Genotypes: *GAL4, UAS-CsChrimson/+*.

986 **Figure 2 – figure supplement 1.** (A-E) Behavior ethograms depict behaviors of
individual larvae displayed in one second bins, scored for 10 sec before, during, and
988 after optical stimulus. Plots depict responses of larvae which contain a single copy of
UAS-CsChrimson together with the indicated *GAL4* driver in the absence and presence
990 of ATR (A-D), or responses of effector-only (*UAS-CsChrimson*/+, ATR+) controls (E).
(F) Plot depicts the fraction of larvae exhibiting indicated behaviors during light stimulus.
992 (G) Latency to the first bend, hunch, back and freeze behaviors following optogenetic
stimulation. Genotypes: *GAL4, UAS-CsChrimson/+*.
994

Figure 3. (A) Optogentic activation of CsChrimson-expressing epidermal cells in the
996 body wall triggers calcium transients in the axon terminal of GCaMP6s-expressing
nociceptive SSNs. Images show responses from one representative animal. Plots depict
998 mean GCaMP6s fluorescence intensity of the axon terminals of (B) C4da, (C) C3da, (D)
Cho, and (E) C1da neurons following optogenetic activation (light stimulus, yellow box)
1000 of epidermal cells over time. Solid lines depict mean GCaMP6s fluorescence across
replicates (n=15 larval fillet preparations), shading indicates SEM, red traces are *GAL4+*
1002 ATR+, blue traces are *GAL4+* ATR-, black trace is *GAL4-* ATR+. (F) The fraction of
larvae exhibiting indicated behaviors during optogenetic epidermal stimulation in
1004 combination with SSN silencing via Tetanus Toxin (TnT) expression. We note that
although baseline rolling probability is elevated in all genetic backgrounds containing
1006 the *AOP-LexA-TnT* insertion, silencing C4da and C3da neurons significantly attenuates
responses to epidermal stimuluation. (G) The duration of the behavioral responses

1008 during optogenetic epidermal stimulation with neuronal TnT expression. Genotypes: (A-
B) *R27H06-LexA* (C4da neurons), *AOP-GCaMP6s, UAS-CsChrimson/+; R38F11-*
1010 *GAL4/+* or *R27H06-LexA* (C4da neurons), *AOP-GCaMP6s, UAS-CsChrimson/+* (*GAL4-*
ATR- effector-only control); (C) *AOP-GCaMP6s, UAS-CsChrimson/+; R38F11-*
1012 *GAL4/NompC-LexA* (C3da neurons); (D) *UAS-GCaMP6s, AOP-CsChrimson, R61D08-*
GAL4 (Cho neurons)*/R38F11-LexA*; (E) *UAS-GCaMP6s, AOP-CsChrimson, R11F05-*
1014 *GAL4* (C1da neurons)*/R38F11-LexA*; (F-G) *R38F11-GAL4, UAS-CsChrimson, AOP-*
LexA-TnT/+ (*Epi>CsChrimson*); *R38F11-GAL4, UAS-CsChrimson, AOP-LexA-TnT/ppk-*
1016 *LexA* (*Epi>CsChrimson + C4da>TnT*); *R38F11-GAL4, UAS-CsChrimson, AOP-LexA-*
TnT/NompC-LexA (*Epi>CsChrimson + C3da>TnT*).
1018

Figure 3 – figure supplement 1. Related to Figure 3A-3D. GCaMP6s responses in
1020 axon terminals of (B) C4da, (C) C3da, (D) Cho and (E) C1da neurons following
optogenetic activation (light stimulus, yellow box) of epidermal cells over time. Each
1022 trace represents the GCaMP6s fluorescence of an individual larval fillet. Red traces are
GAL4+ ATR+, blue traces are *GAL4+* ATR-, black trace is *GAL4-* ATR+. Genotypes: (A)
1024 *R27H06-LexA*, *AOP-GCaMP6s, UAS-CsChrimson/+; R38F11-GAL4/+* or *R27H06-*
LexA, *AOP-GCaMP6s, UAS-CsChrimson/+* (*GAL4*-ATR- effector-only control); (B)
1026 *AOP-GCaMP6s, UAS-CsChrimson/+; R38F11-GAL4/NompC-LexA*; (C) *UAS-*
GCaMP6s, AOP-CsChrimson, R61D08-GAL4 /R38F11-LexA; (D) *UAS-GCaMP6s,*
1028 *AOP-CsChrimson, R11F05-GAL4/R38F11-LexA*.

1030 **Figure 3 – figure supplement 2**. Related to Figure 3E-3F. (A-C) Behavior ethograms
(left) and fraction of larvae (right) exhibiting indicated behaviors to optogenetic
1032 epidermal stimulation in combination with (A) an *AOP-TNT* transgene (control lacking
LexA driver), (B) C4da neuron silencing via Tetanus Toxin (TnT), and (C) C3da neuron
1034 silencing via TnT. (D) Fraction of larvae exhibiting each behavior and (E) the duration of
behavior responses after removal of the light stimulus. Genotypes are indicated in (A-
1036 C).

1038 **Figure 4.** Epidermal stimulation augments nociceptive responses. (A) Mean GCaMP6s
responses (F/F_0) in C4da axons during optogenetic stimulation (yellow box) of C4da
1040 neurons alone (green) or of C4da neurons and epidermal cells (magenta), shading
indicates SEM. (B) Simultaneous epidermal stimulation increased the peak calcium
1042 response (F_{max}/F_0), (C) total calcium influx (area under the curve), and (D) duration of
C4da neuron calcium responses compared to stimulation of C4da neurons alone.
1044 Genotypes: *ppk-LexA, AOP-GCAMP6s/+; R27H06-GAL4/UAS-CsChrimson* (C4da) and
ppk-LexA, AOP-GCAMP6s/+; R27H06-GAL4/R38F11-GAL4, UAS-CsChrimson
1046 (C4da+epi). (E-J) Characterization of the behavioral responses to low-intensity
optogenetic stimulation of C4da neurons, epidermal cells, or simulteanous C4da
1048 neurons and epidermal cells. (E) Cumulative and (F) total roll probability during
optogenetic stimulation (indicated by the red bar). n = 33 (*C4da>CsChrimson*), 30
1050 (*Epi>CsChrimson*), and 31 (*C4da + Epi>CsChrimson*) larvae. (G, H) Number and
frequency distribution of rolls, (I) latency to the first roll observed for larvae of the
1052 indicated genotypes, and (J) the duration of the indicated behaviors during light
stimulus. Genotypes: *UAS-CsChrimson/+; R27H06-GAL4/+* (C4da), *UAS-*
1054 *CsChrimson/+; R38F11-GAL4/+* (Epidermis), *UAS-CsChrimson/+; R27H06-*
GAL4/R38F11-GAL4 (C4da+Epidermis). (K) Roll probability of larvae to a 20 mN or 50
1056 mN von Frey mechanical stimulus and epidermal optogenetic activation (a light
stimulus, 30mW/cm^2 that was insufficient on its own to induce nocifensive rolling).
1058 Larvae were reared in the presence or absence of ATR, as indicated. Genotypes: *UAS-*
CsChrimson/+; R38F11-GAL4/+. (L-N) Prior epidermal but not nociceptor stimulus
1060 potentiates mechanical nociceptive responses. (L) Roll probability of control larvae
(*UAS-TrpA1/+*) or larvae expressing TrpA1 in the epidermis (*Epi-GAL4: R38F11-GAL4)*
1062 or C4da neurons (*UAS-TrpA1/+*; *C4da-GAL4 #1: R27H06-GAL4, UAS-TrpA1/+*; *C4da-*
GAL4 #2: ppk-GAL4, UAS-TrpA1/+), or control larvae (*no GAL4: UAS-TrpA1/+*;) in
1064 response to 40 mN mechanical stimulus 10 sec following 10 sec of a thermal stimulus
(25° or 32° C). To control for effects of genetic background, we confirmed that each of
1066 the experimental genotypes exhibited mechanically induced nociceptive sensitization
(Fig. 4S1C). (M) Roll probability of control larvae (*UAS-TrpA1/+*) or larvae expressing

1068 TrpA1 in the epidermis (*Epi>TrpA1*: *R38F11-GAL4, UAS-TrpA1/+*) in response to a 40
mN mechanical stimulus delivered at the indicated time interval following a 32º C
1070 thermal stimulus. (N) Nociceptive enhancement (difference in the roll probablity to the
first and second stimulus) is plotted against the recovery duration and results were fit to
1072 an exponential curve to derive the decay time constant. The red line indicates
nociceptive enhancement of a mechanical stimulus by a prior epidermal thermogenetic
1074 stimulus; the black line indicates nociceptive enhancement by a prior mechanical
stimulus.
1076

Figure 4 – figure supplement 1. (A) GCaMP6s responses (F/F_0) of individual
1078 replicates during optogenetic stimulation (yellow box) of C4da neurons alone (green) or
C4da neurons and epidermal cells (magenta), yellow box indicates presence of light
1080 stimulus. Genotypes: *ppk-LexA, AOP-GCAMP6s/+; R27H06-GAL4/UAS-CsChrimson*
(C4da) and *ppk-LexA, AOP-GCAMP6s/+; R27H06-GAL4/R38F11-GAL4, UAS-*
1082 *CsChrimson* (C4da+epi). (B) Roll probability of larvae in response to two successive 40
mN mechanical stimuli spaced by the indicated amount of time (recovery duration).
1084 Genotype: *R38F11-GAL4/+*. (C) Roll probability of larvae expressing *UAS-TrpA1* in
nociceptors exhibited levels of mechanically induced nociceptive potentiation
1086 comparable to other experimental genotypes used in the study (control*: UAS-TrpA1/+*;
epidermis*: R38F11-GAL4, UAS-TrpA1/+*; nociceptors*: R27H06-GAL4, UAS-TrpA1/+*).
1088

Figure 5. Epidermal cells are intrinsically mechanosensitive. (A) Schematic of
1090 preparation to measure radial stretch evoked calcium responses of dissociated
epidermal cells. (B) Representative calcium responses of a dissociated epidermal cell to
1092 0.5% and 1% radial stretch (successive stimuli), 2.5% radial stretch, and 5% radial
stretch. (C) Dose response curve displaying the fraction of epidermal cells activated by
1094 increasing magnitudes of stretch. Red trace displays the mean ± SEM across six
independent dissociated cell preparations, obtained from a minimum of 6 larvae. Gray
1096 traces display fraction responding in each dissociated cell preparation replicate. (D)
Subsets of epidermal cells display varying stretch thresholds, n = 6 dissociated cell

1098 preparations, for a total of 654 epidermal cells. (E) Representative mechanically induced epidermal calcium responses in the larval body wall. Images show GCaMP6s
1100 fluorescence intensity 100 msec prior to (i) and 20 sec following (ii) a 25 μm membrane displacement (poke). (F) Distribution of the peak calcium response (F_{max}/F_0) to a 25 μm
1102 membrane displacement (poke) of 24 cells from 24 independent larval fillets. Cells were classified as responders (>10% increase in normalized GCaMP6s fluorescence). (G)
1104 Mean calcium responses (F/F_0) of poke responders and non-responders (n = 12 cells each). Solid lines depict mean normalized GCaMP6s fluorescence and shading
1106 indicates SEM. Genotype: *R38F11-GAL4, UAS-GCaMP6s*.

1108 **Figure 5 – figure supplement 1.** Subsets of epidermal cells display calcium responses to diverse mechanical stimuli. Representative calcium traces of epidermal cells that
1110 respond to: (A) laminar flow via perfusion, (B) laminar flow and osmotic stretch, (C) 15% hypo-osmotic stretch, and (D) 30% hypo-osmotic stretch, or (E) do not respond to either
1112 flow or stretch. (F) Proportion of epidermal cells that are sensitive to mechanical stimuli. n = three distinct cell preparations, 6 larvae per preparation, for a total of 177 cells. (G)
1114 Related to Figure 5G. GCaMP6s responses (F/F_0) of individual epidermal cells to a 25 μm membrane displacement. Genotype: *R38F11-GAL4, UAS-GCaMP6s*.

1116 **Figure 6**. CRAC channels are required for epidermal mechanosensory responses and epidermal nociceptive potentiation. (A) RNAi screen for epidermal ion channels required
1118 for mechanically induced nociceptive potentiation. Bars depict nociceptive potentiation index (difference in the larval roll probability to the first and second mechanical stimuli
1120 divided by roll probability to the first mechanical stimulus). Candidate channels were chosen for further analysis if they had a a z-score greater than 2 (absolute value). (B)
1122 The CRAC channels Orai and Stim are required in epidermal cells for mechanically evoked nociceptive potentiation. Roll probability of larvae of the indicated genotypes
1124 (Control RNAi, *R38F11-GAL4, UAS-RFP-RNAi/+*; *Stim* RNAi, *R38F11-GAL4, UAS-Stim-RNAi/+*; *Orai* RNAi, *R38F11-GAL4, UAS-Orai-RNAi/+*) to a 40 mN mechanical
1126 stimulus followed by a second 40mN mechanical stimulus 10 sec later. (C) *Drosophila*

epidermal cells display classical store-operated calcium entry (SOCE). Treatment with
1128 the drug thapsigargin (TG) in the absence of extracellular calcium promoted depletion of intracellular calcium stores and calcium influx, following extracellular calcium re-
1130 addition. (D) Like TG, 1% stretch in the absence of extracellular calcium induced depletion of intracellular calcium stores and calcium influx, following extracellular
1132 calcium re-entry. (E) 69% of stretch responsive cells displayed greater calcium influx during intracellular calcium stores release than during the calcium re-entry phase. (F-G)
1134 The Orai blocker, lanthanum chloride (500 nM) or the depletion of intracellular stores by thapsigargin (1 μM) reduces the fraction of stretch-sensitive epidermal cells. (H-I) The
1136 fraction of stretch-sensitive epidermal cells is significantly decreased in cells isolated from larvae expressing *Stim* RNAi, or *Orai* RNAi, as compared to control RNAi. (J)
1138 Stretch stimuli evoke dose-dependent calcium signals in the human keratinocyte HaCaT cell line. (K) Representative stretch-evoked SOCE calcium response in HaCaT cells.
1140 Stretch induces calcium release from stores in the absence of extracellular calcium and a greater calcium influx in the presence of extracellular calcium. (L) Epidermal
1142 hyperpolarization enhances mechanical nocifensive responses. Roll probability of larvae expressing GtACR in epidermal cells (*R38F11-GAL4, UAS-GtACR/+*) or control larvae
1144 (*R38F11-GAL4/+*) to a single 70 mN mechanical stimulus. (M) Epidermal *Stim* overexpression enhances mechanical nocifensive responses. Roll probability of *Stim*-
1146 overexpressing larvae (*R38F11-GAL4, UAS-Stim/+*) and control larvae (*R38F11-GAL4/+*) to two successive 40 mN mechanical stimuli delivered 10 sec apart. (N)
1148 Epidermal potentiation of mechanical nociceptive responses requires exocytosis. Roll probability of control larvae (*UAS-shi^{ts}/+*) or larvae expressing temperature-sensitive
1150 dominant-negative shibire in epidermal cells (*R38F11-GAL4, UAS-shi^{ts}/+*) in response to two successive mechanical stimuli that followed 10 min of conditioning at the
1152 permissive (25° C) or non-permissive (30° C) temperature. (O) Model of epidermal-neuronal signaling. Mechanically evoked Stim/Orai calcium signaling in epidermal cells
1154 drives calcium influx and vesicle release that drives nociceptor activation and mechanical sensitization via activation of C4da nociceptors.
1156

Figure 6 – figure supplement 1. Related to Figure 6A. Ion channel expression in
1158 epidermal cells. Five populations of *UAS-GFP*-expressing epidermal cells were selected
for RNA-seq analysis. GFP-positive epidermal cells were dissociated into single cell
1160 suspensions, manually picked, and subjected to RNA-Seq analysis. Plots depict
expression levels (mean +/- standard deviation) of the indicated ion channels
1162 (log_2(TPM+1)) from n > 6 independent libraries for each sample type.
(A) Expression in epidermal cells collected from *R38F11-GAL4* which labels all
1164 epidermal cells. (B) Anatomically defined subsets of epidermal cells were profiled by
removing posterior segments from *R38F11-GAL4, UAS-GFP* larvae (*R38F11-GAL4*
1166 head and thorax) or (C) dissecting the ventral epidermis (*R38F11-GAL4* ventral
epidermis). (D) Expression in the dorsal epidermis (*ush-GAL4*) and or (E) bands of
1168 epidermal cells (*R51F10-GAL4).*

1170 **Figure 6 – figure supplement 2**. (A-B) Epidermal knockdown of ion channels affects
larval mechanical nociceptive responses. Roll probability in response to the first and
1172 second mechanical stimulus for larvae expressing RNAi transgenes to (A) *Orai* or
attP40 RNAi control transgene and (B) *Task6* or *attP2* RNAi control transgene. (C)
1174 Epidermal cell SOCE is attenuated by pre-treatment with the Orai blocker, lanthanum
chloride (100 nM). (D) Representative SOCE after treatment with TG (1 μM) in
1176 epidermal cells isolated from larvae treated with control RNAi, *Stim* RNAi (red), or *Orai*
RNAi, (blue). (E) Peak calcium response following SOCE in epidermal cells isolated
1178 from larvae treated with control RNAi, *Stim* RNAi (red), or *Orai* RNAi, (blue). (F) *Stim*
RNAi decreases calcium store content of epidermal cells. Calcium store content was
1180 measured as the area under the curve of the cytosolic calcium response to TG (1 μM) in
the absence of extracellular calcium.

Details of Statistical Analysis

Figure 1C: Fisher's exact test with BH correction

UAS-TRPA1 groups (25 C vs 32 C)	p-value	q-value	Significance (q<0.05)
Control (no *GAL4* driver)	0.2424	2.424000e-01	F
R27H06-GAL4	2.2e-16	3.666667e-16	T
R38F11-GAL4	2.2e-16	3.666667e-16	T
R38F11-GAL4 + elav-GAL80	2.2e-16	3.666667e-16	T
R38F11-GAL4 + tshGAL80	4.111e-15	5.138750e-15	T

Figure 1S4: ANOVA with post-hoc Tukey's test

Dendrite length	p-value	Significance
R38 vs. UAS-luc RNAi	>0.9999	F
R38 vs. UAS-CsChrimson	0.9659	F
R38 vs. UAS-TRPA1	0.9982	F
R38 vs. UAS-orai RNAi	0.9009	F
R38 vs. UAS-Stim RNAi	0.9219	F
R38 vs. UAS-Stim	>0.9999	F
R38 vs. UAS-shi^TS	0.9974	F

Dendrite branchpoints	p-value	Significance
R38 vs. UAS-luc RNAi	0.9945	F
R38 vs. UAS-CsChrimson	0.9269	F
R38 vs. UAS-TRPA1	0.6859	F
R38 vs. UAS-orai RNAi	0.9896	F
R38 vs. UAS-Stim RNAi	0.9949	F
R38 vs. UAS-Stim	0.8654	F
R38 vs. UAS-shi^TS	>0.9999	F

Figure 1S6C: Fisher's exact test

	p-value	Significance
rolling	0.0002928	T
c-bend	2.035e-10	T
backing	0.0008424	T
hunch	0.004233	T
freeze	0.002342	T

Figure 1S6D: Wilcoxon rank sum test

	p-value	Significance
rolling	Cannot compare	
c-bend	0.8907	F
backing	0.00127	T
hunch	Cannot compare	
freeze	Cannot compare	

Figure 2F: Wilcoxon Rank-Sum test

	p-value	Significance
C4da vs Epi	0.0067	T

Figure 2G: Kruskal-Wallis test followed by Wilcoxon rank sum test with BH correction

	p-value	q-value	Significance (q<0.05)

Kruskal-Wallis test, rolling	N/A (only epi + C4da have values)		
rolling C4da vs Epi	0.03124		T
Kruskal-Wallis test, c-bend	0.0001652		T
c-bend C4da vs Epi	0.001468	0.002936	T
c-bend C3da vs Epi	0.3237	0.323700	F

Figure 2H Fisher's exact test with a BH correction

	p-value	q-value	Significance (q<0.05)
rolling Epi ATR+ vs ATR-	0.04313	0.09102	F
rolling C4da ATR+ vs ATR-	0.04551	0.09102	F
rolling C3da ATR+ vs ATR-	1	1	F
rolling Cho ATR+ vs ATR	1	1	F
c-bend Epi ATR+ vs ATR-	0.4687	0.9508	F
c-bend C4da ATR+ vs ATR-	0.4754	0.9508	F
c-bend C3da ATR+ vs ATR	1	1	F
c-bend Cho ATR+ vs ATR	1	1	F
back Epi ATR+ vs ATR-	0.00000000000004556	0.00000000000018224	T
back C4da ATR+ vs ATR	1	1	F
back C3da ATR+ vs ATR	1	1	F
back Cho ATR+ vs ATR-	0.1128	0.2256	F
hunch Epi ATR+ vs ATR	1	1	F
hunch C4da ATR+ vs ATR	1	1	F
hunch C3da ATR+ vs ATR-	1	1	F
hunch Cho ATR+ vs ATR-	0.4918	1	F
freeze Epi ATR+ vs ATR-	0.00000008682	0.00000034728	T
freeze C4da ATR+ vs ATR-	0.4754	0.6338667	F
freeze C3da ATR+ vs ATR-	1	1	F
freeze Cho ATR+ vs ATR-	0.000825	0.00165	T

Figure 2S1E: Fisher's exact test with BH correction

	p-value	q-value	Significance (q<0.05)
rolling Epi ATR+ vs ATR-	3.039e-06	6.0780e-06	T
rolling C4da ATR+ vs ATR-	9.667e-08	3.8668e-07	T
rolling C3da ATR+ vs ATR-	1	1.0000e+00	F
rolling Cho ATR+ vs ATR-	1	1.0000e+00	F
c-bend Epi ATR+ vs ATR-	1.388e-11	2.776e-11	T
c-bend C4da ATR+ vs ATR-	1.265e-11	2.776e-11	T
c-bend C3da ATR+ vs ATR-	0.00192	2.560e-03	T
c-bend Cho ATR+ vs ATR-	1	1.000e+00	F
back Epi ATR+ vs ATR-	1.238e-13	4.952000e-13	T
back C4da ATR+ vs ATR-	0.6003	6.003000e-01	F
back C3da ATR+ vs ATR-	0.02597	5.194000e-02	F
back Cho ATR+ vs ATR-	0.05251	7.001333e-02	F
hunch Epi ATR+ vs ATR-	0.04313	5.750667e-02	F
hunch C4da ATR+ vs ATR-	0.4754	4.754000e-01	F
hunch C3da ATR+ vs ATR-	1.03e-06	2.060000e-06	T
hunch Cho ATR+ vs ATR-	2.571e-14	1.028400e-13	T
freeze Epi ATR+ vs ATR-	0.01869	0.0747600	F
freeze C4da ATR+ vs ATR-	0.2219	0.2958667	F
freeze C3da ATR+ vs ATR-	0.5353	0.5353000	F
freeze Cho ATR+ vs ATR-	0.05251	0.1050200	F

Figure 3E Fisher's exact test with BH correction

	p-value	q-value	Significance (q<0.05)
rolling control vs *C4da>TNT*	0.001051	0.002102	T
rolling control vs *C3da>TNT*	0.1945	0.194500	F
c-bend control vs *C4da>TNT*	1	1.00000	F
c-bend control vs *C3da>TNT*	0.05219	0.10438	F
back control vs *C4da>TNT*	0.7787	0.778700	F
back control vs *C3da>TNT*	0.005579	0.011158	T
hunch control vs *C4da>TNT*	0.02372	0.04744	T
hunch control vs *C3da>TNT*	0.1124	0.11240	F
freeze control vs *C4da>TNT*	0.3533	0.3533	F
freeze control vs *C3da>TNT*	0.1945	0.3533	F

Figure 3F Kruskal-Wallis test followed by Wilcoxon rank sum test with BH correction

	p-value	q-value	Significance (q<0.05)
Kruskal-Wallis test, rolling	0.0004424		
rolling control vs *C4da>TNT*	0.001122	0.002244	T
rolling control vs *C3da>TNT*	0.7007	0.700700	F
Kruskal-Wallis test, c-bend	0.001948		
c-bend control vs *C4da>TNT*	0.0004278	0.0008556	T
c-bend control vs *C3da>TNT*	0.433	0.4330000	F
Kruskal-Wallis test, back	0.4203		
back control vs *C4da>TNT*	N/A		
back control vs *C3da>TNT*	N/A		
hunch control vs *C4da>TNT*	No Hunch in control		
hunch control vs C3da TNT	No Hunch in control (p=0.4127 C4vsC3)		
Kruskal-Wallis test, freeze	0.3808		
freeze control vs *C4da>TNT*	N/A		
freeze control vs *C3da>TNT*	N/A		

Figure 3S2 D: Fisher's exact test with BH correction

	p-value	q-value	Significance (q<0.05)
Control vs C4da silence, roll	0.0003682	0.0007364	T
Control vs C3da silence, roll	0.3015	0.3015000	F
Control vs C4da silence, c-bend	0.1188	0.2376	F
Control vs C3da silence, c-bend	0.2949	0.2949	F
Control vs C4da silence, backward	1	1.00000	F
Control vs C3da silence, backward	0.02372	0.04744	T
Control vs C4da silence, hunch	1	1	F
Control vs C3da silence, hunch	1	1	F
Control vs C4da silence, freeze	0.1028	0.102800	F
Control vs C3da silence, freeze	0.002466	0.004932	T

Figure 3S2 E: Kruskal-Wallis test followed by Wilcoxon rank sum test

	p-value	q-value	Significance
Kruskal-Wallis test, Roll	0.02471		T
Control vs C4da silence Roll	0.01604	0.03208	T
Control vs C3da silence Roll	0.04658	0.04658	T
Kruskal-Wallis test, c-bend	0.01971		T
Control vs C4da silence c-bend	0.008927	0.017854	T
Control vs C3da silence c-bend	0.02334	0.023340	T

Control vs C4da silence back	0.2222		F
Control vs C3da silence back	N/A		
Control vs C3da silence back	N/A		
Control vs C4da silence hunch	N/A		
Control vs C3da silence hunch	N/A		
Control vs C4da silene freeze	N/A		
Control vs C3da silence freeze	N/A		

Figure 4B: Wilcoxon Rank-Sum test

	p-value	Significance
Fmax/F0 C4da vs C4da +Epi	0.0288	T

Figure 4C: Wilcoxon Rank Sum test

	p-value	q-value	Significance (q<0.05)
C4da vs C4da+Epi	0.03184		T

Figure 4D: Wilcoxon Rank-Sum test

	p-value	Significance
C4da vs C4da+Epi	0.03277	T

Figure 4F: Fisher's exact test with BH correction

	p-value	q-value	Significance (q<0.05)
C4da vs Epi	0.0003136	3.741e-04	T
C4da vs Epi+C4da	0.7541	3.741e-04	T
Epi vs Epi+C4da	0.000005162	2.997e-11	T

Figure 4G: Kruskal-Wallis test followed by Wilcoxon rank sum test with BH correction

	p-value	q-value	Significance (q<0.05)
Kruskal-Wallis test	0.000000001544		
C4da vs Epi	0.7541	0.7541	F
C4da vs Epi+C4da	0.000000000001072	0.000000000003216	T
Epi vs Epi+C4da	0.000005162	0.000007743	T

Figure 4H: Fisher's exact test with BH correction

	p-value	q-value	Significance (q<0.05)
<5 C4da vs Epi	0.1894	1.894e-01	F
<5 C4da vs C4da+Epi	3.646e-11	5.469e-11	T
<5 Epi vs C4da+Epi	2.571e-14	7.713e-14	T
5-9 C4da vs Epi	0.674	0.674	F
5-9 C4da vs C4da+Epi	0.356	0.674	F
5-9 Epi vs C4da+Epi	0.6124	0.674	F
10 -14 C4da vs Epi	0.6144	0.9216	F
10 -14 C4da vs C4da+Epi	1	1.0000	F
10 -14 Epi vs C4da+Epi	0.6124	0.9216	F
15 -19 C4da vs Epi	1	1.0000	F
15-19 C4da vs C4da+Epi	0.1896	0.2844	F
15 -19 Epi vs C4da+Epi	0.1128	0.2844	F
>20 C4da vs Epi	1	1.0000	F
>20 C4da vs C4da+Epi	5.377e-11	1.6131e-10	T
>20 Epi vs C4da+Epi	2.644e-10	3.9660e-10	T

Figure 4I: Kruskal-Wallis test followed by Wilcoxon rank sum test with BH correction

	p-value	q-value	Significance (q<0.05)
Kruskal-Wallis test	5.993e-15		
C4da vs Epi	0.0009667	9.6670e-04	T
C4da vs Epi+C4da	4.97e-15	7.4550e-15	T
Epi vs Epi+C4da	5.028e-16	1.5084e-15	T

Figure 4J: Kruskal-Wallis test followed by Wilcoxon rank sum test with BH correction

	p-value	q-value	Significance (q<0.05)
Kruskal-Wallis test, rolling	4.024e-09		T
roll C4da vs Epi	0.1937	1.9370e-01	F
roll C4da vs C4da+Epi	9.024e-12	2.7072e-11	T
roll Epi vs C4da + Epi	5.506e-05	8.2590e-05	T
Kruskal-Wallis test, c-bend	0.06175		F
c-bend C4da vs Epi	N/A		
c-bend C4da vs C4da+Epi	N/A		
c-bend Epi vs C4da +Epi	N/A		
Kruskal-Wallis test, backing	9.145e-06		T
back C4da vs Epi	9.574e-07	2.8722e-06	T
back C4da vs C4da+Epi	0.02662	2.6620e-02	T
back Epi vs C4da+Epi	0.001987	2.9805e-03	T
Kruskal-Wallis test, hunching	0.006437		T
hunch C4da vs Epi	0.2706	0.270600	F
hunch C4da vs C4da+Epi	0.001252	0.003756	T
hunch Epi vs C4da+Epi	0.1836	0.270600	F
Kruskal-Wallis test, freezing	0.4857		F
freeze C4da vs Epi	N/A		
freeze C4da vs C4da+Epi	N/A		
freeze Epi vs C4da+Epi	N/A		

Figure 4K: Fisher's exact test with a BH correction

Epi-GAL4, UAS-CsChrimson treatment groups	p-value	q-value	Significance
20 mN ATR- vs ATR+ Epi>CsChrimson	0.003234	0.0097020	T
50 mN ATR- vs ATR+ Epi>CsChrimson	0.008797	0.0131955	T
50mN ATR- vs ATR+ CsChrimson	0.7639	0.7639000	F

Figure 4L: Fisher's exact test with BH correction

	p-value	q-value	Significance (q<0.05)
No *GAL4* 25 vs 32	0.6798	0.7806000	F
Epi-GAL4 25 vs 32	0.0005454	0.0021816	T
27H06-GAL4 25 vs 32	0.7806	0.7806000	F
ppk-GAL4 25 vs 32	0.7735	0.7806000	F

Figure 4M: Fisher's exact test with BH correction

UAS-TRPA1 comparisons	p-value	q-value	Significance (q<0.05)
10sec control vs 10sec *Epi-GAL4*	0.006108	0.01018000	T
30sec control vs 30sec *Epi-GAL4*	0.001265	0.00316250	T
60sec control vs 60sec *Epi-GAL4*	0.00007129	0.00035645	T
300sec control vs 300sec *Epi-GAL4*	0.07531	0.09413750	F
600sec control vs 600sec *Epi-GAL4*	0.4351	0.43510000	F

Figure 4N: Curve fitting

	fit curve	Decay time constant
Mechano (Fig 4S1B)	f(x) = 0.4139*exp(-0.002994*x)	334.001336
Epidermal activation (Fig 4L)	f(x) = 0.47*exp(-0.002964*x)	337.3819163

Figure 4S1B: Fisher's exact test with BH correction

	p-value	q-value	Significance (q<0.05)
10sec 1st vs 2nd	0.0007546	0.0018865	T
30sec 1st vs 2nd	0.000006865	0.000034325	T
60sec 1st vs 2nd	0.008544	0.01424	T
300sec 1st vs 2nd	0.131	0.16375	F
600sec 1st vs 2nd	0.3217	0.3217	F

Figure 4S1C: Fisher's exact test with BH correction

	p-value	q-value	Significance (q<0.1)
Control 1st vs 2nd	0.006746	0.00674600	T
Epi-GAL4 1st vs 2nd	6.336e-05	0.00019008	T
Nociceptor-GAL4 1st vs 2nd	0.005186	0.00674600	T

Figure 6B Fisher's exact test with BH correction

	p-value	q-value	Significance (q<0.1)
Control 1st vs 2nd	4.94E-05	0.0002472	T
Orai RNAi 1st vs 2nd	0.1329	0.3236667	F
Stim RNAi 1st vs 2nd	0.1942	0.3236667	F
Control 1st vs *Orai* RNAi 1st	0.8788	0.6660000	F
Control 1st vs *Stim* RNAi 1st	0.5328	0.8788000	F

Figure 6E: Chi-square comparing distribution of stretch sensitive cells

	Chi-square value	DF	p-value
Control vs *Stim* RNAi	33	4	<0.0001
Control vs *Orai* RNAi	150.6	4	<0.0001
Stim RNAi vs *Orai* RNAi	3.689	4	0.4497

Figure 6G: Chi-square comparing distribution of stretch sensitive cells

	Chi-square value	DF	p-value
Control vs La3+	36.09	4	<0.0001
Control vs Store Depleted	112.1	4	<0.0001
Store Depleted vs La3+	40.69	4	<0.0001

Figure 6J: Fisher's exact test

	p-value		
control vs *GtACR*	0.03216		

Figure 6K Fisher's exact test with BH correction

	p-value	q-value	Significance (q<0.1)
Control 1st vs 2nd	0.00037	0.00148000	T
Stim OE 1st vs 2nd	0.02386	0.03181333	T
Control 1st vs *Stim OE* 1st	0.002115	0.00423000	T

Figure 6L: Fisher's exact test with BH correction

	p-value	q-value	Significance
Control 25C 1st vs Control 25C 2nd	5.425e-05	7.233333e-05	T
Control 30C 1st vs Control 30C 2nd	1.033e-06	2.066000e-06	T
Epi>shi 25C 1st vs *Epi>shi* 25C 2nd	4.912e-07	1.964800e-06	T
Epi>shi 30C 1st vs *Epi>shi* 30C 2nd	0.05076	5.076000e-02	F

Figure 6S2A Fisher's exact test with BH correction

	p-value	q-value	significance
Control Trial 1 vs Trial 2	0.002438	0.004876	T
Orai RNAi Trial 1 vs Trial 2	0.4076	0.4076	F

Figure 6S2B Fisher's exact test with BH correction

	p-value	q-value	significance
Control Trial 1 vs Trial 2	0.00157	0.003140	T
Task6 RNAi Trial 1 vs Trial 2	0.004795	0.004795	T

Figure 6S2C Wilcoxon Rank-Sum test

	p-value	significance
Control vs La^{3+} block	0.0003377	T

Figure 6S2E: Kruskal-Wallis test followed by Wilcoxon rank sum test with BH correction

	p-value	q-value	Significance (q<0.05)
Kruskal-Wallis test	0.00001332		T
Control vs *Stim* RNAi	0.0009161	0.001374150	T
Control vs *Orai* RNAi	0.000005094	0.000015282	T
Stim RNAi vs *Orai* RNAi	0.3759	0.375900000	F

Figure 6S2F: Kruskal-Wallis test followed by Wilcoxon rank sum test with BH correction

	p-value	q-value	Significance (q<0.05)
Kruskal-Wallis test	0.004105		T
Control vs *Stim* RNAi	0.001296	0.002592	T
Control vs *Orai* RNAi	0.8294	0.829400	F

Yoshino et al, Fig. 1

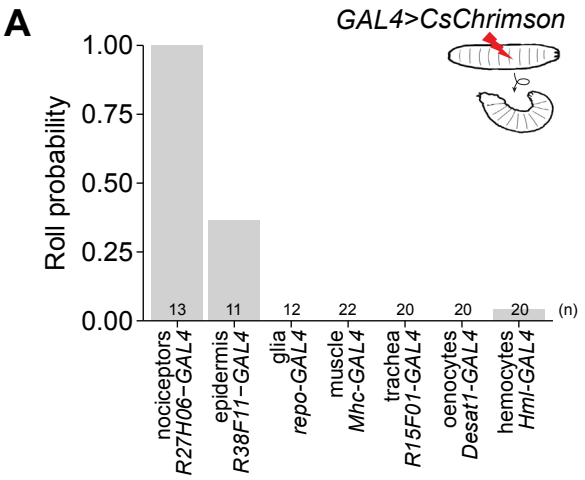

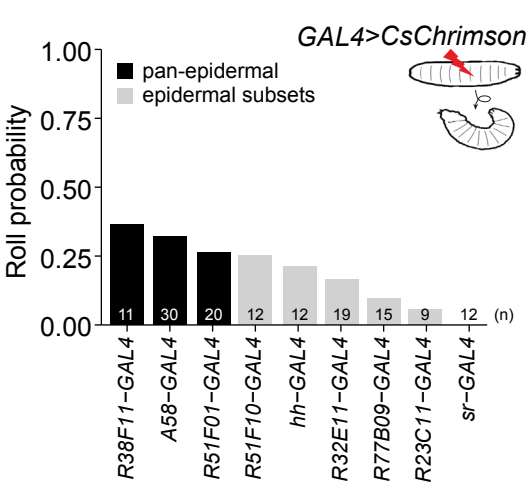

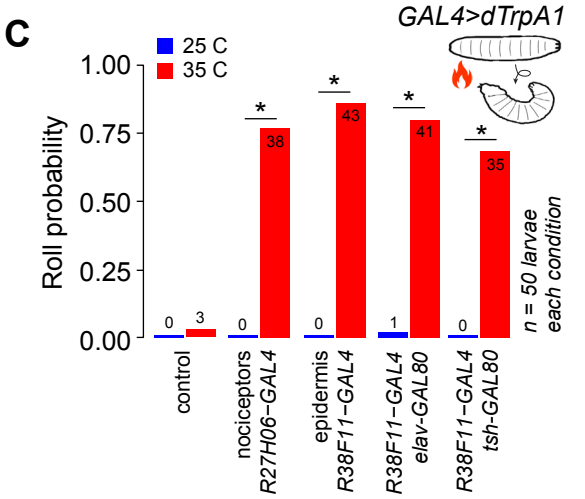

Yoshino et al, Fig. 1S1

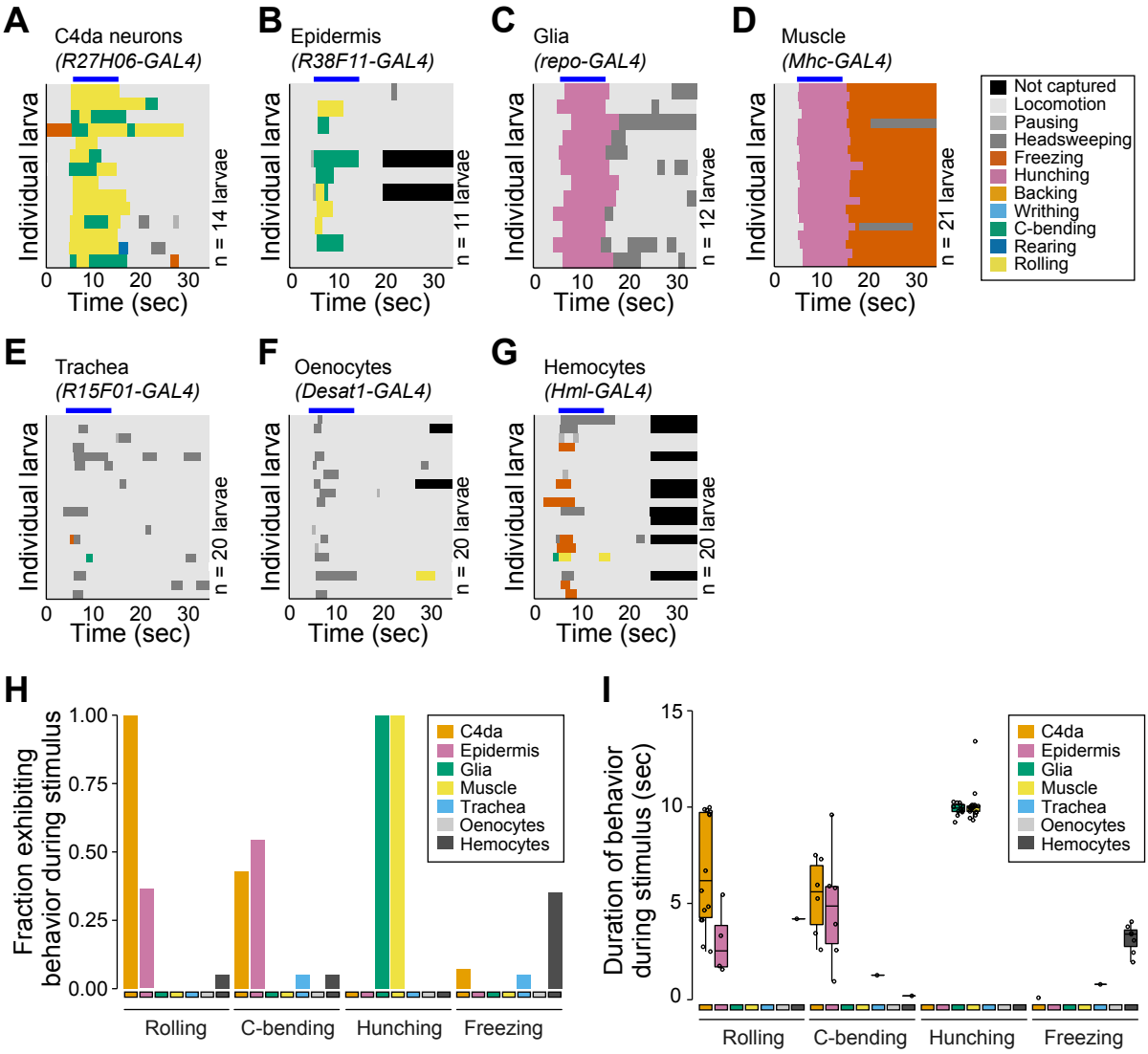

Yoshino et al, Fig. 1S2

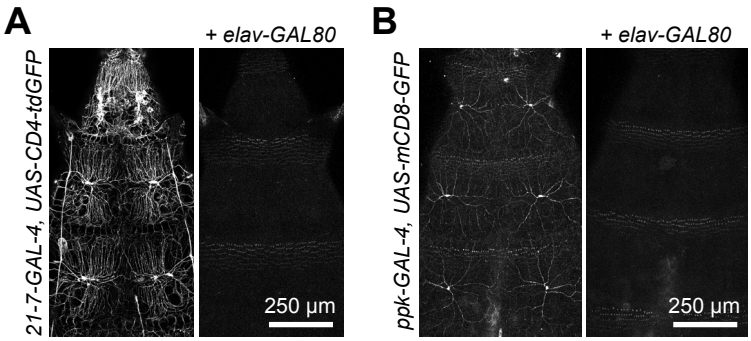

Yoshino et al, Fig. 1S3

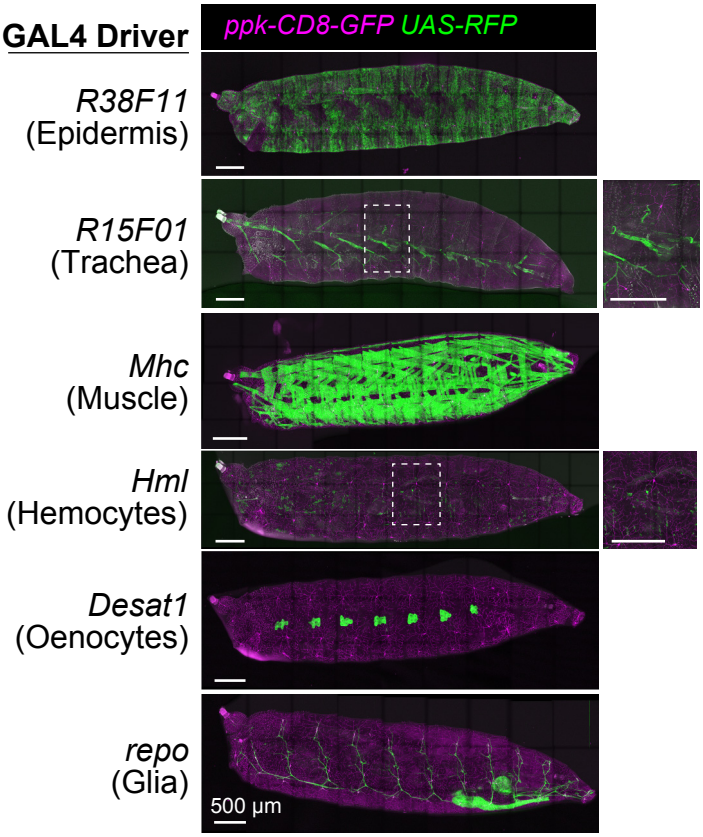

Yoshino et al, Fig. 1S4

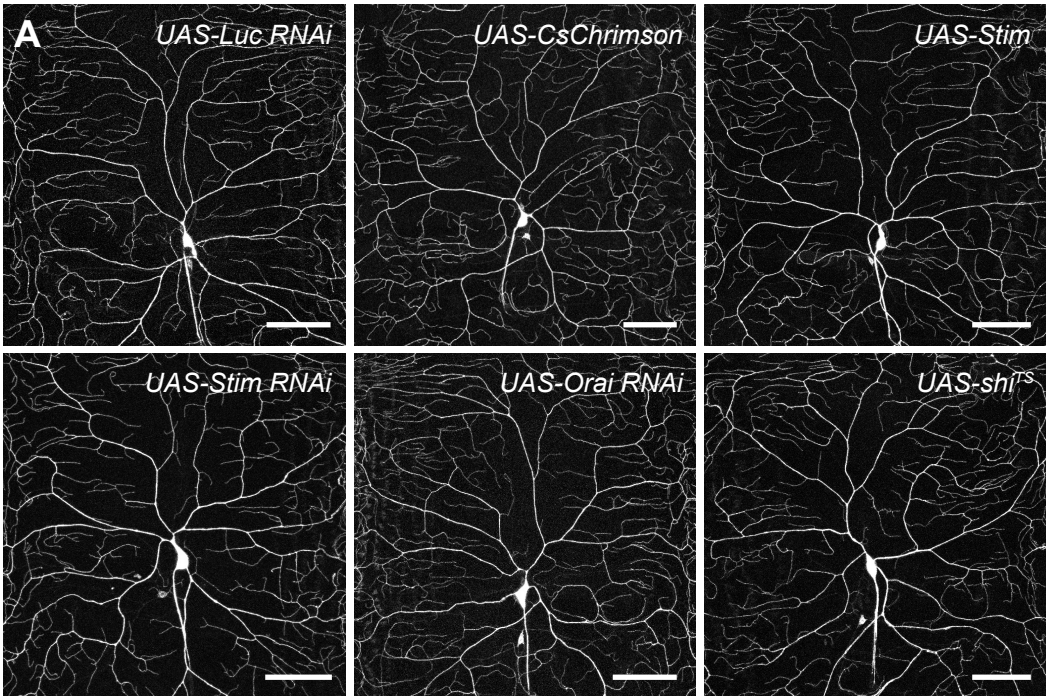

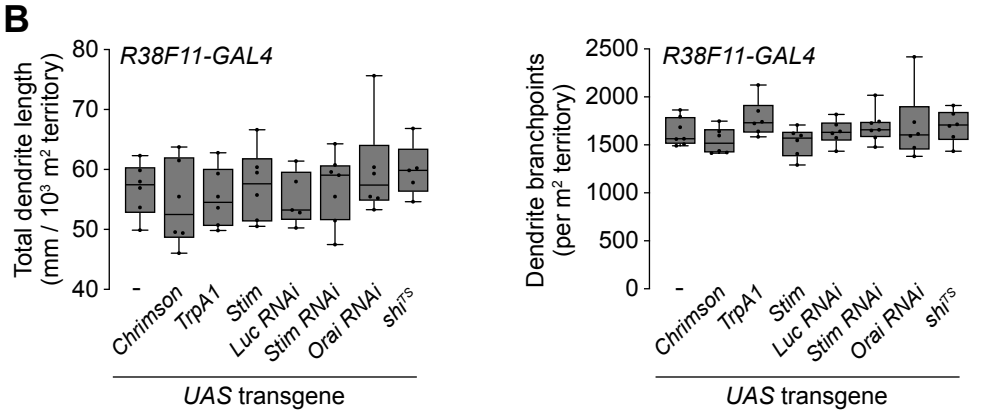

Yoshino et al, Fig. 1S5

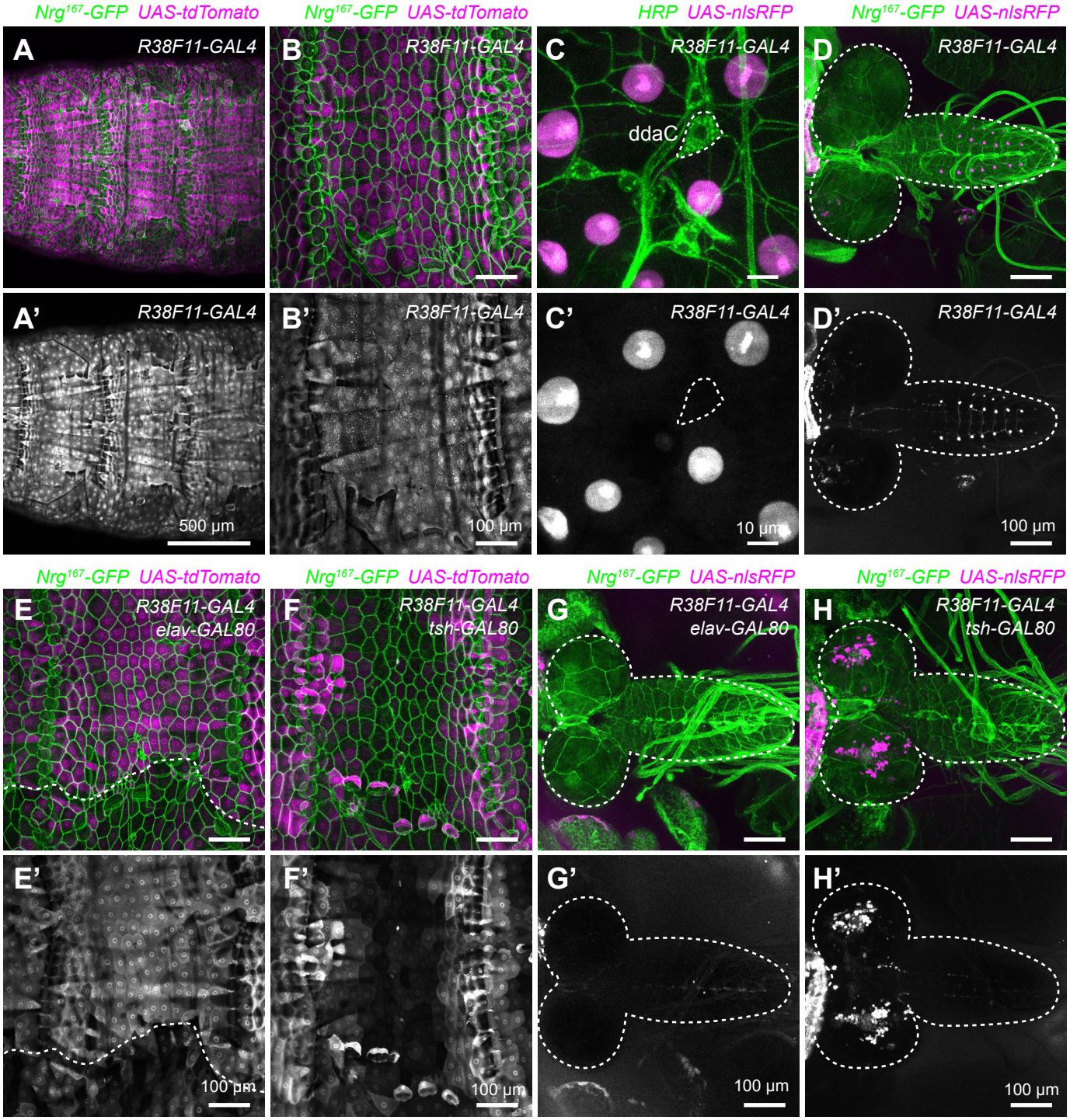

Yoshino et al, Fig. 1S6

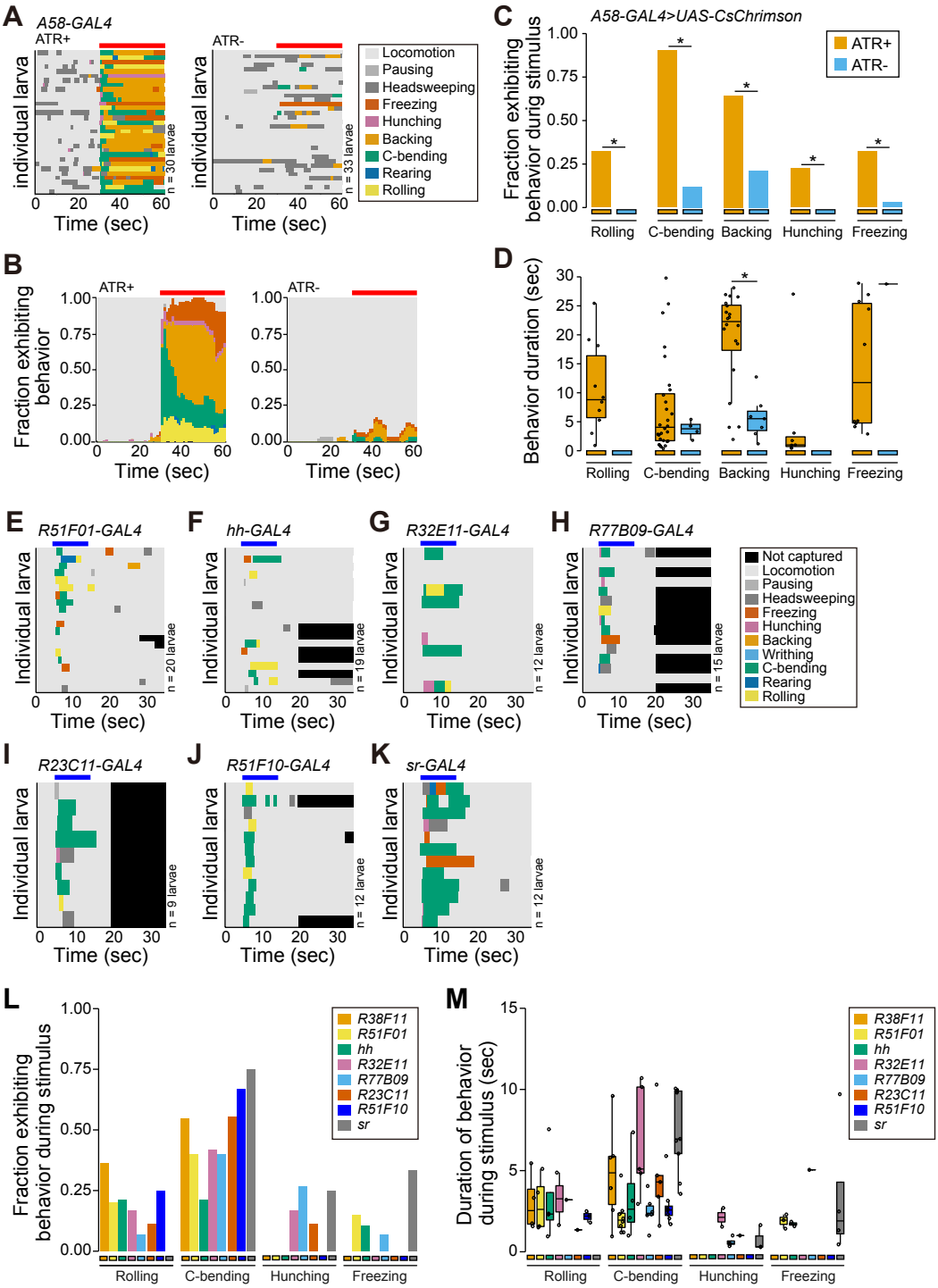

Yoshino et al, Fig. 1S7

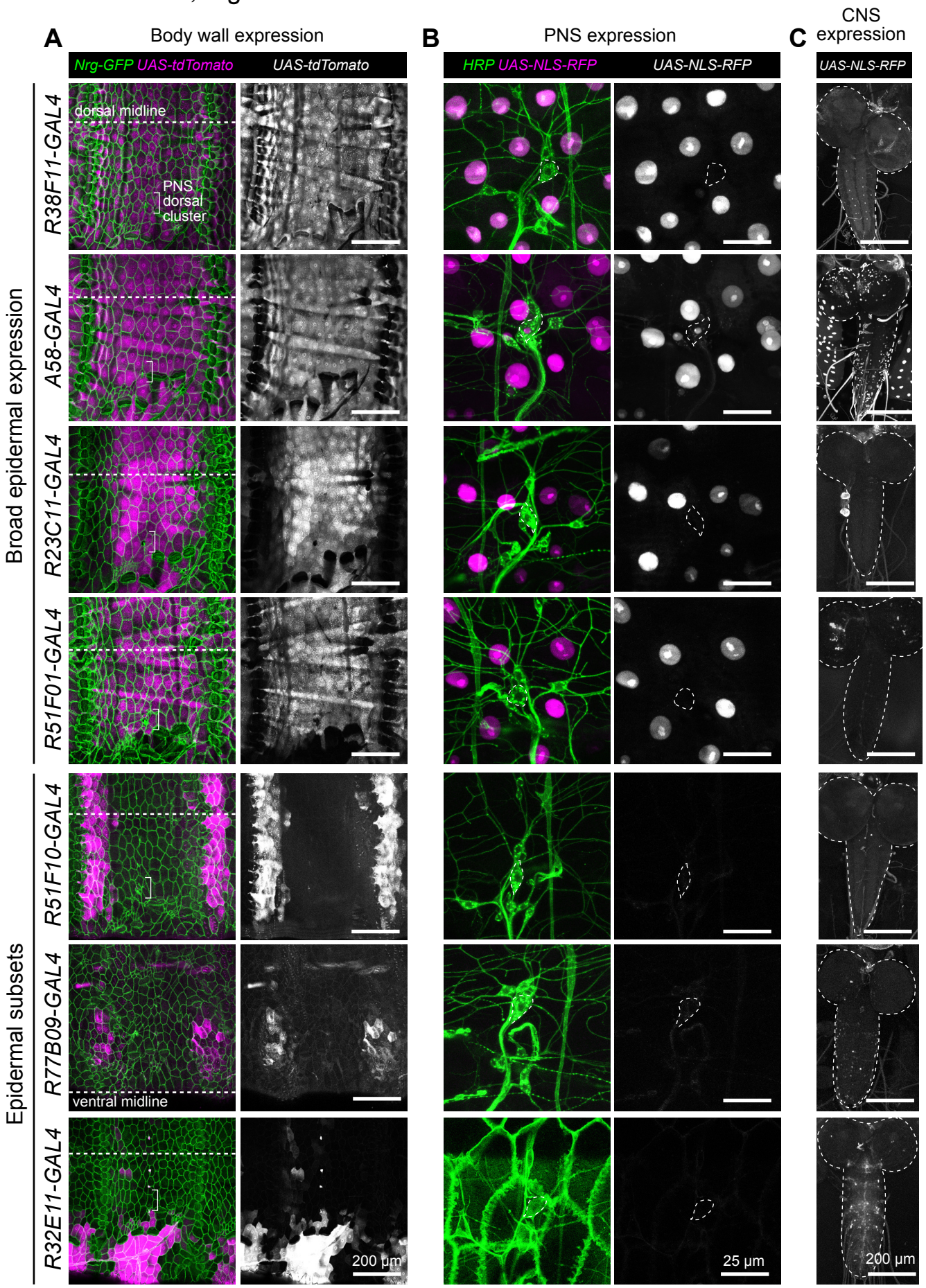

Yoshino et al, Fig. 2

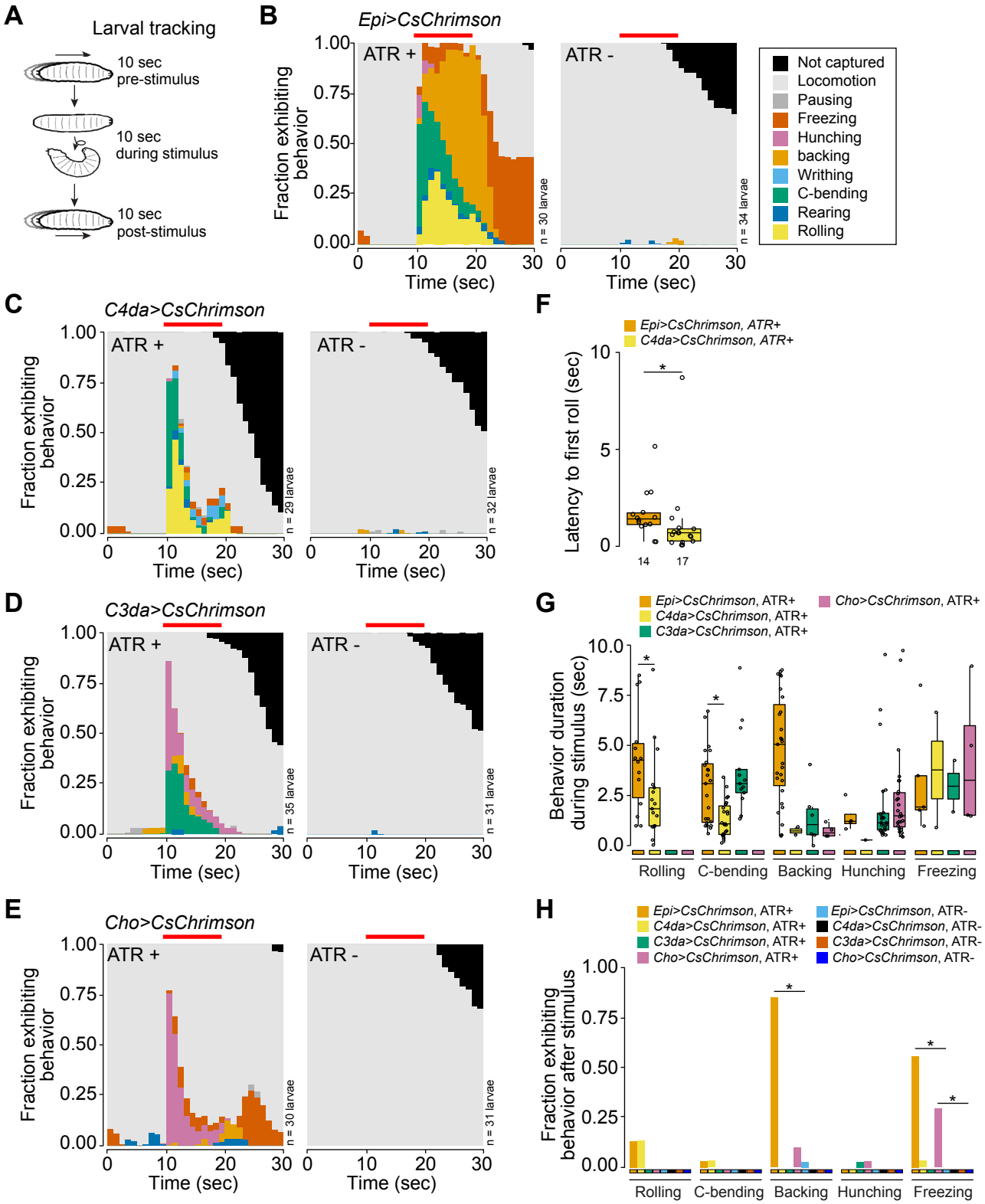

Yoshino et al, Fig. 2S1

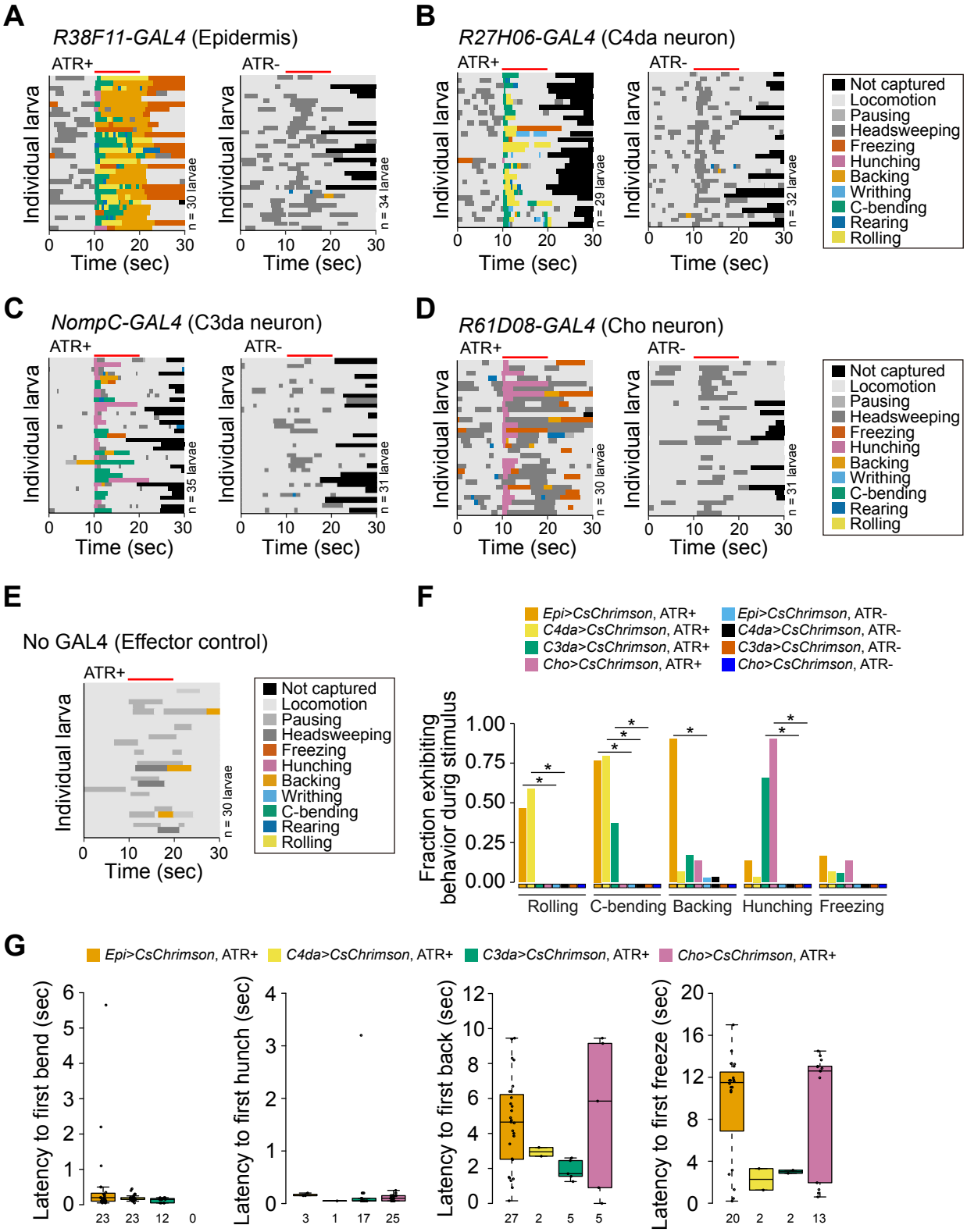

Yoshino et al, Fig. 3

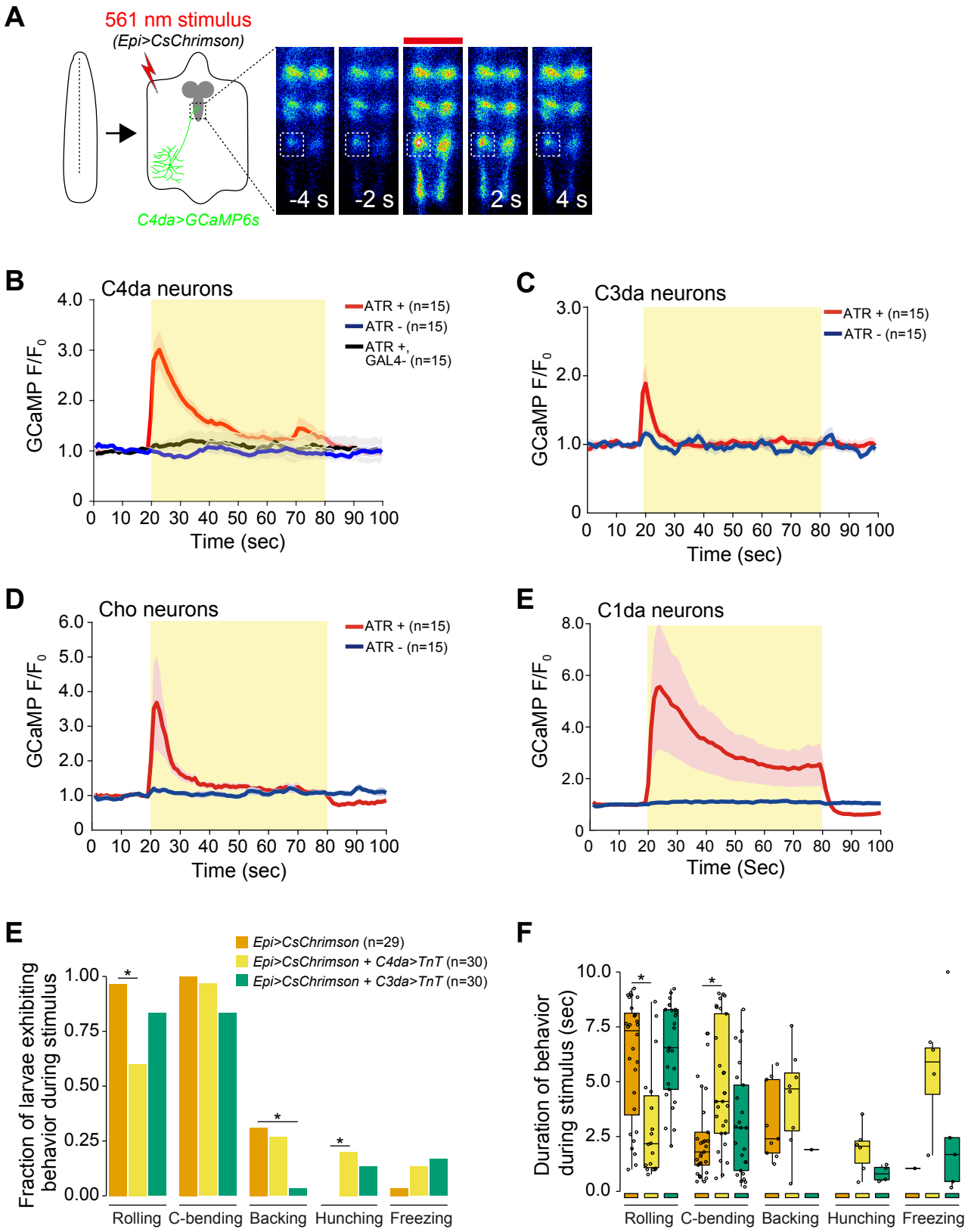

Yoshino et al, Fig. 3S1

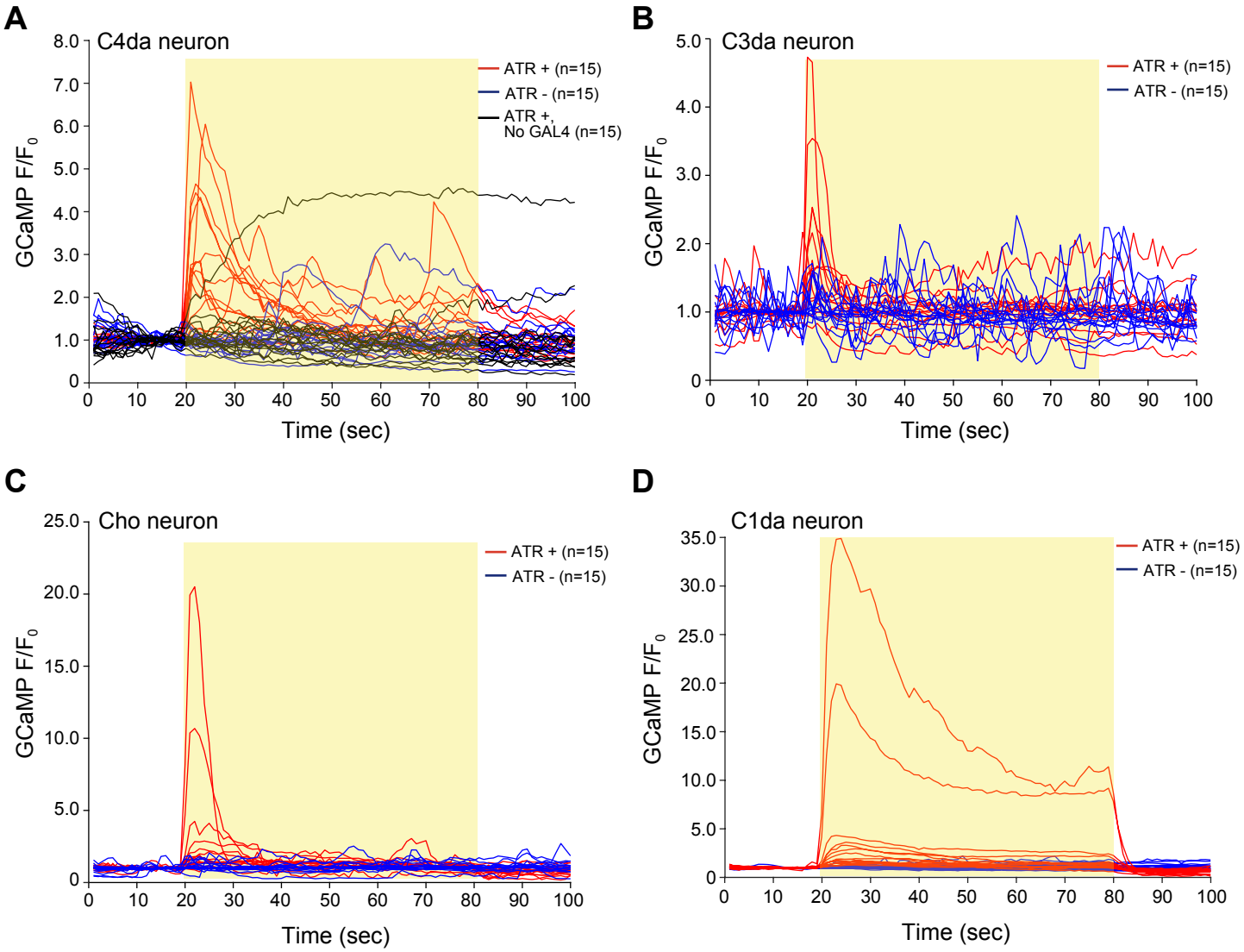

Yoshino et al, Fig. 3S2

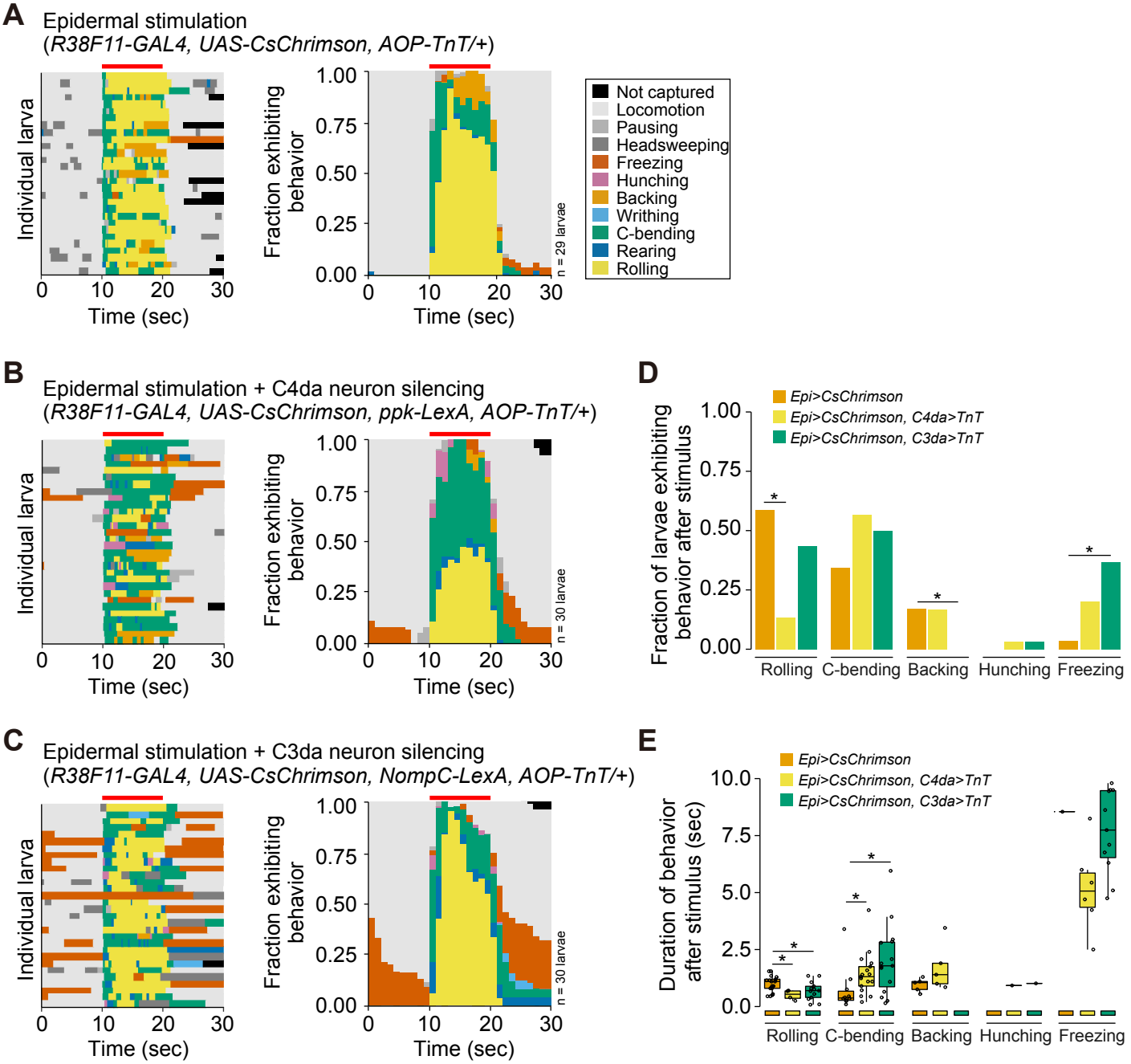

Yoshino et al, Fig. 4

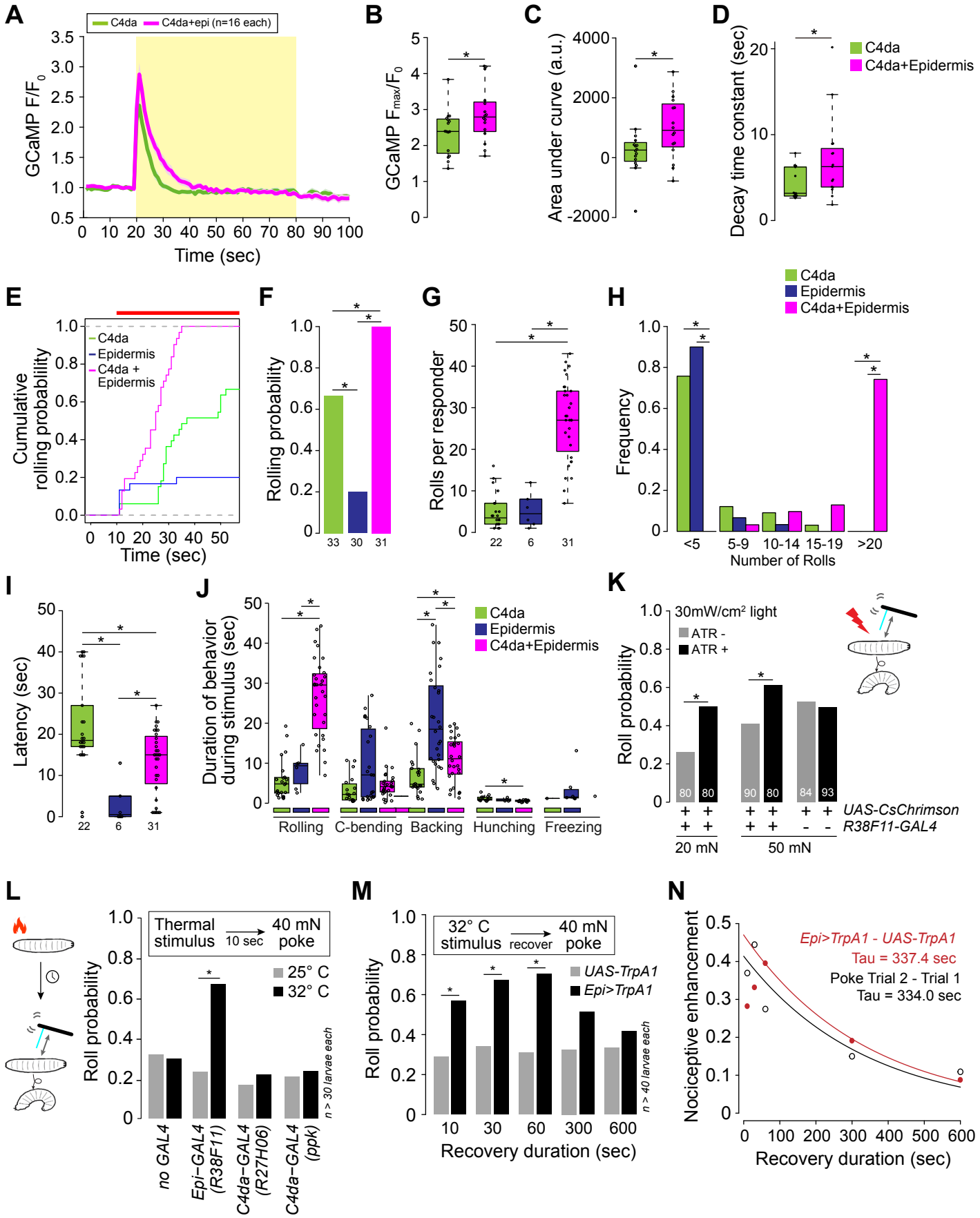

Yoshino et al, Fig. 4S1

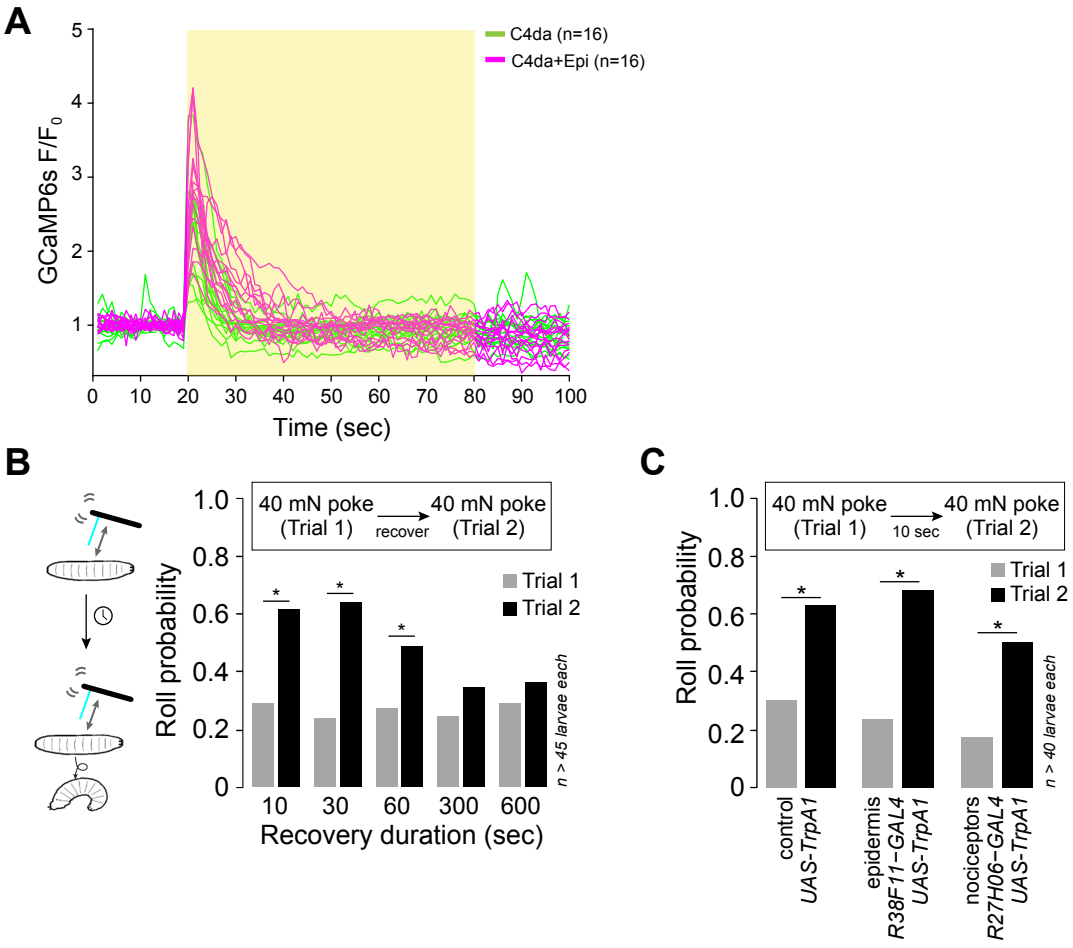

Yoshino et al, Fig. 5

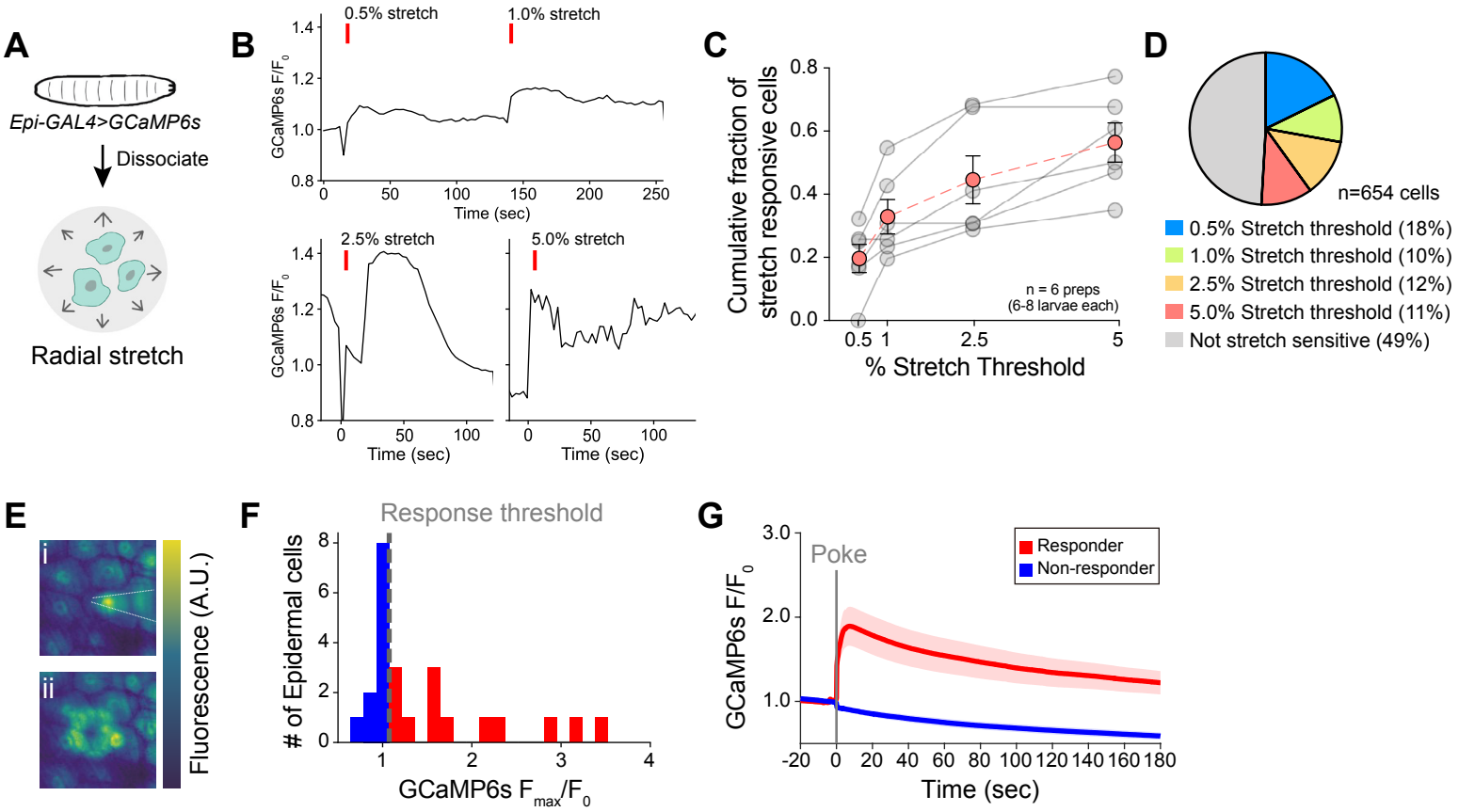

Yoshino et al, Fig. 5S1

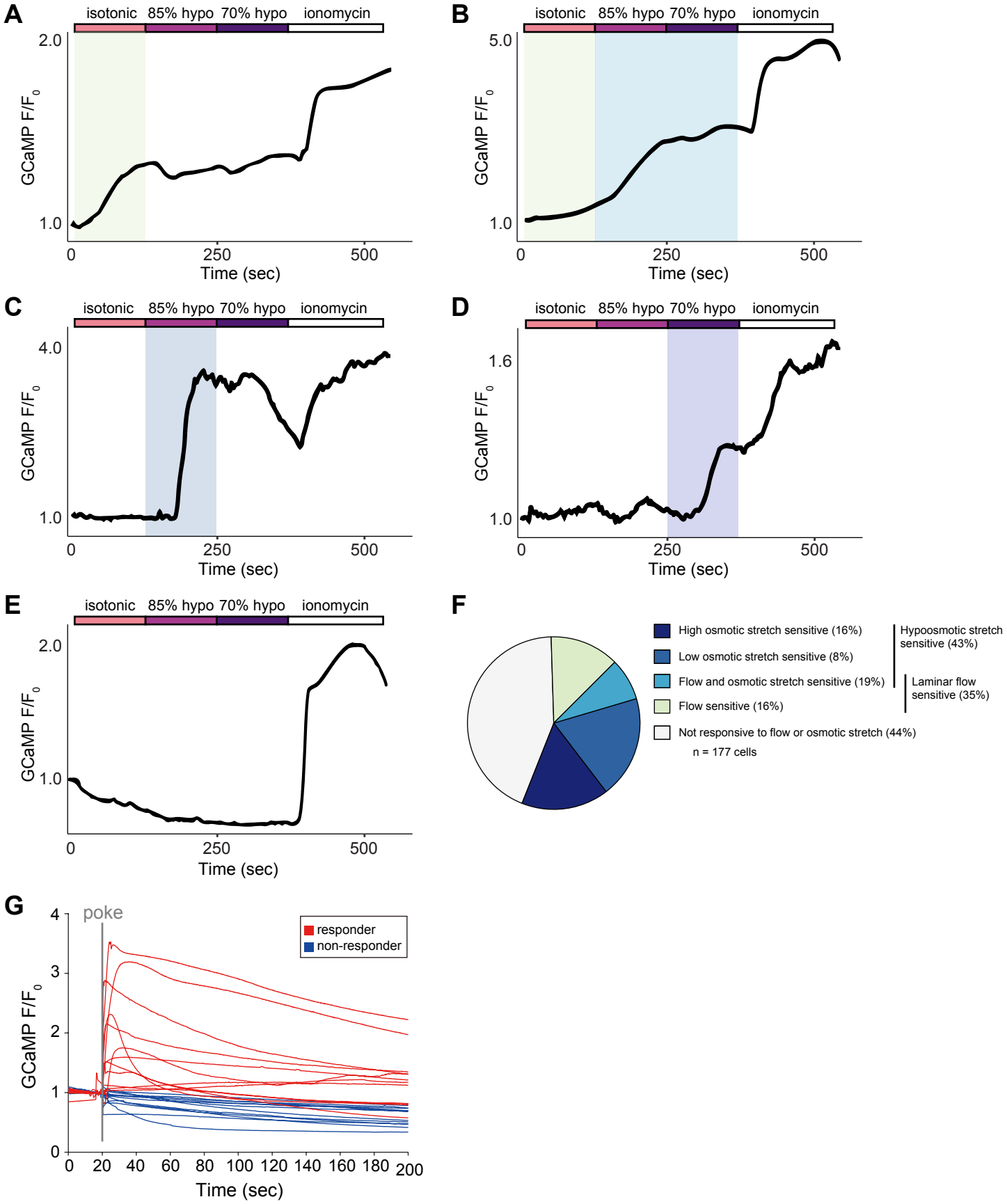

Yoshino et al, Fig. 6

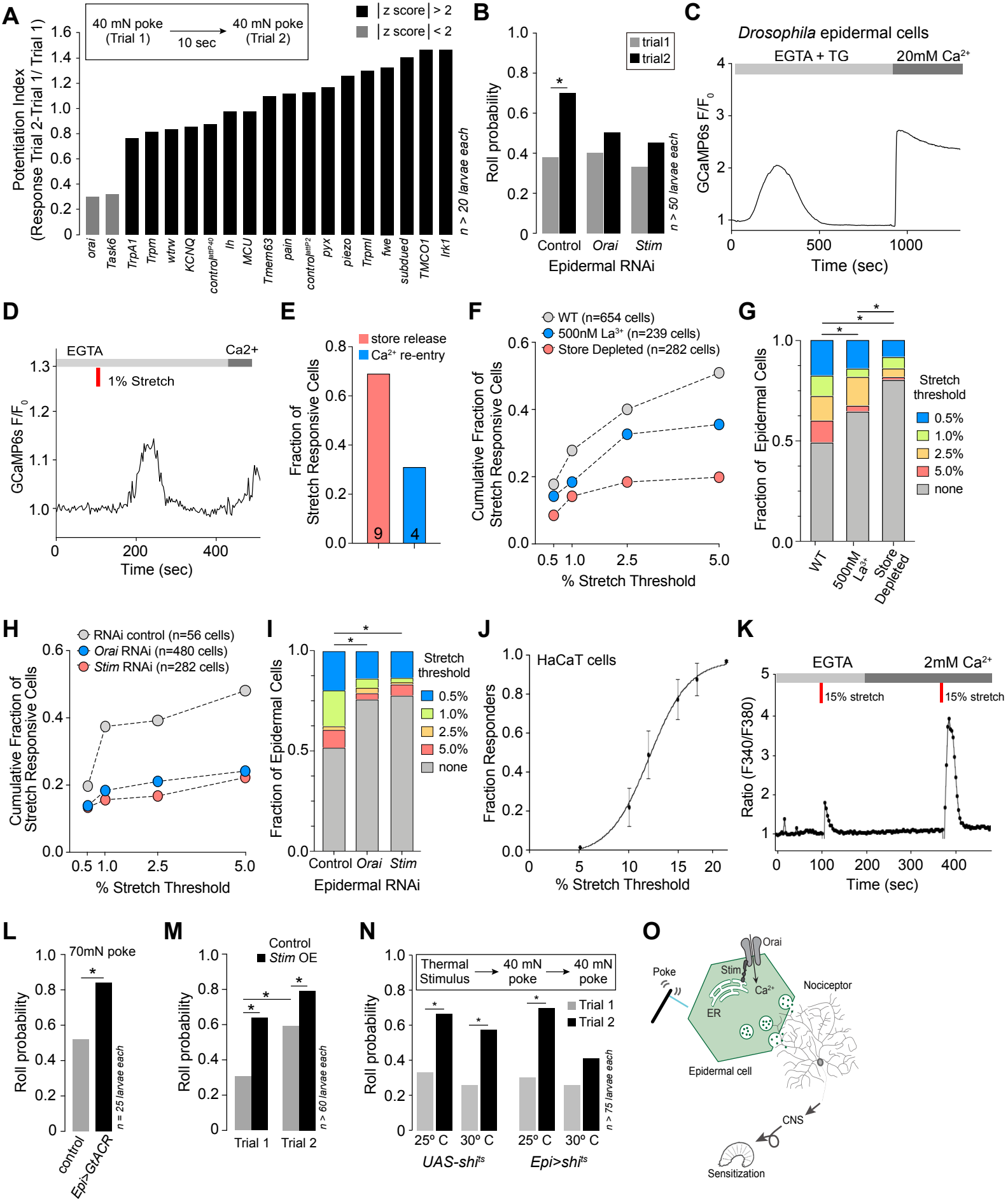

Yoshino et al, Fig. 6S1

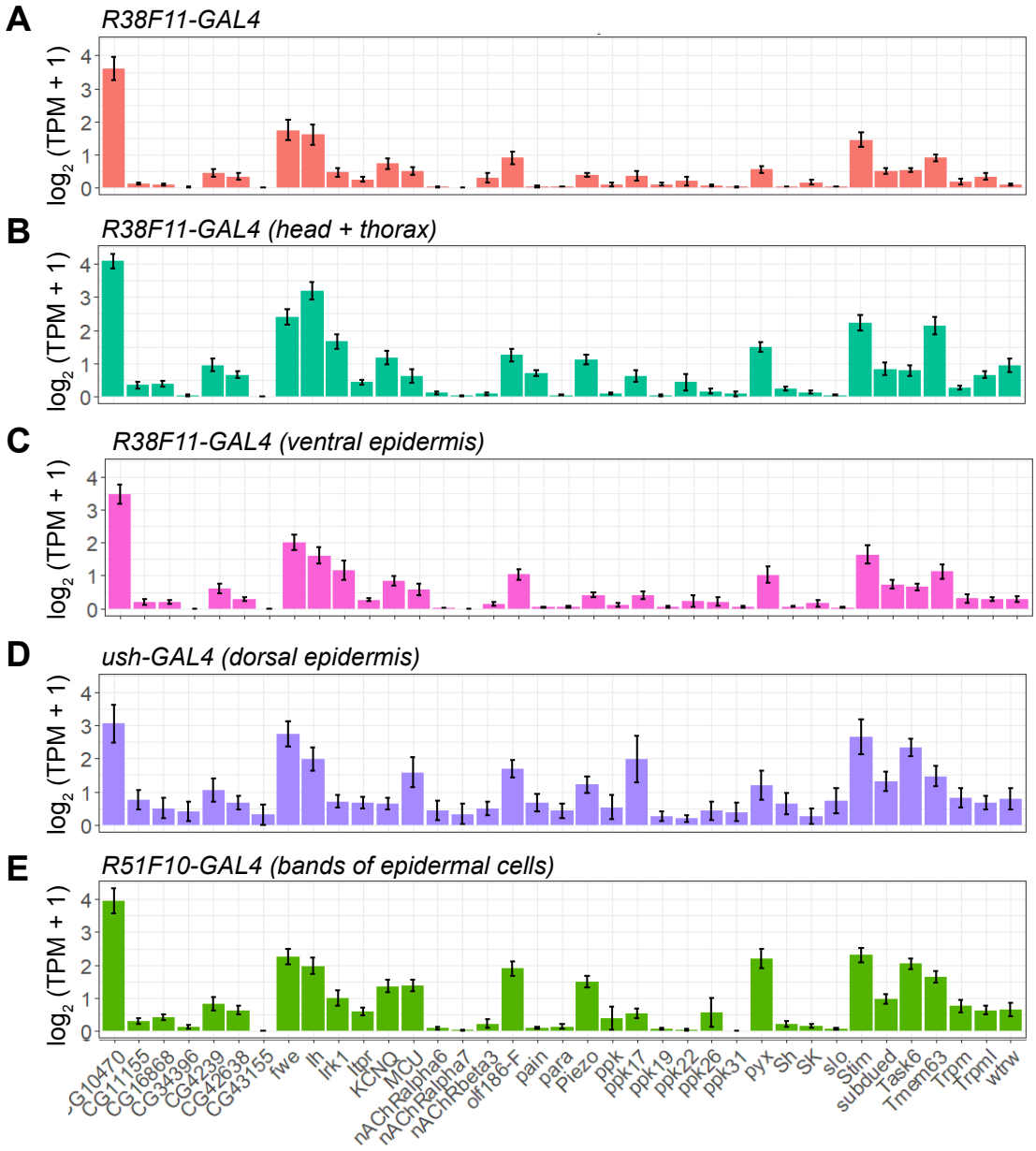

Yoshino et al, Fig. 6S2

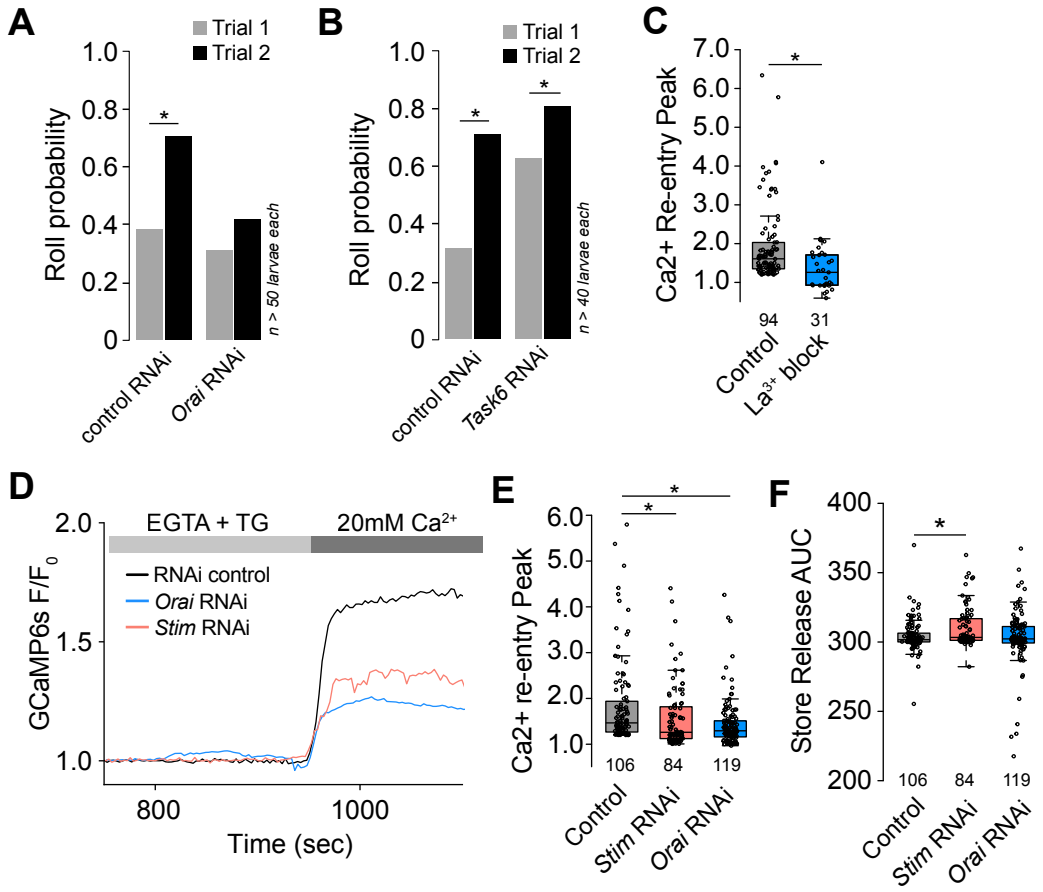

Table S1. Alleles used in this study

Transgene / Allele	Uses / Features	Identifier (RRID)
A58-GAL4	GAL4 driver (epidermis)	Flybase_FBal0181674
Desat1-GAL4	GAL4 driver (oenocytes)	BDSC_65405
GMR15F01-GAL4	GAL4 driver (trachea)	BDSC_45071
GMR23C11-GAL4	GAL4 driver (epidermis)	BDSC_45123
GMR27H06-GAL4	GAL4 driver (C4da neurons)	BDSC_49440
GMR32E11-GAL4	GAL4 driver (epidermis)	BDSC_48109
GMR38F11-GAL4	GAL4 driver (epidermis)	BDSC_50014
GMR51F01-GAL4	GAL4 driver (epidermis)	BDSC_38787
GMR51F10-GAL4	GAL4 driver (epidermis)	BDSC_38793
GMR61D08-GAL4	GAL4 driver (Cho neurons)	BDSC_39272
GMR77B09-GAL4	GAL4 driver (epidermis)	Flybase_FBti0138381
hh-GAL4	GAL4 driver (epidermis)	DGGR_118117
Hml-GAL4	GAL4 driver (hemocytes)	BDSC_6395
MHC-GAL4	GAL4 driver (muscle)	BDSC_55132
NompC-GAL4	GAL4 driver (C3da neurons)	BDSC_36361
Piezo-GAL4	GAL4 driver (Piezo-expressing cells)	BDSC_78335
ppk-GAL4	GAL4 driver (C4da neurons)	BDSC_32079
21-7-GAL4	GAL4 driver (MD neurons)	Flybase_FBti0131369
repo-GAL4	GAL4 driver (glia)	BDSC_7415
sr-GAL4	GAL4 driver (apodemes)	BDSC_26663
ppk-LexA	LEXA driver (C4da neurons)	Flybase_FBtp0125814
NompC-LexA	LEXA driver (C3da neurons)	BDSC_52241
elav-GAL80	GAL80 (pan-neuronal)	Flybase_FBtp0079702
tsh-GAL80	GAL80 (VNC)	Flybase_FBti0114123
ush-GAL4	GAL4 driver (epidermis)	BDSC_36524
Nrg167GFP	Reporter (epidermal cell junctions)	BDSC_6844
UAS-tdTomato	Reporter (RFP)	BDSC_36328
UAS-RedStinger	Reporter (NLS-RFP)	BDSC_8546
UAS0GCaMP6s	Reporter (Calcium indicator)	BDSC_42749
UAS-GCaMP6s	Reporter (Calcium indicator)	BDSC_42746
AOP-GCaMP6s	Reporter (Calcium indicator)	BDSC_44273
AOP-TNT	Neuronal silencing (Tetanus Toxin)	Flybase_FBtp0144631
UAS-shi-ts	Inducible inhibition of endocytosis	BDSC_44222
UAS-CsChrimson	Inducible Cation Channel	BDSC_55135
UAS-CsChrimson	Inducible Cation Channel	BDSC_55136
UAS-TRPA1	Inducible Cation Channel	BDSC_26263
UAS-GtACR	Inducible Anion Channel	BDSC_92983
UAS-luciferase RNAi	RNAi transgene	BDSC_31603
UAS-RFP-RNAi	RNAi transgene	BDSC_67852
UAS-fwe-RNAi	RNAi transgene	BDSC_27323
UAS-Ih-RNAi	RNAi transgene	BDSC_29574
UAS-Ih-RNAi	RNAi transgene	BDSC_58089

UAS-Irk1-RNAi	RNAi transgene	BDSC_42644
UAS-KCNQ-RNAi	RNAi transgene	BDSC_80446
UAS-MCU-RNAi	RNAi transgene	BDSC_67897
UAS-orai-RNAi	RNAi transgene	BDSC_53333
UAS-orai-RNAi	RNAi transgene	VDRC_12221
UAS-pain-RNAi	RNAi transgene	BDSC_51835
UAS-piezo-RNAi	RNAi transgene	FlyBase_FBst0457216
UAS-piezo-RNAi	RNAi transgene	Flybase_FBtp0071516
UAS-pyx-RNAi	RNAi transgene	BDSC_31297
UAS-stim-RNAi	RNAi transgene	BDSC_41759
UAS-stim-RNAi	RNAi transgene	FlyBase_FBst0478081
UAS-subdued-RNAi	RNAi transgene	FlyBase_FBst0480747
UAS-Task6-RNAi	RNAi transgene	BDSC_28016
UAS-Task6-RNAi	RNAi transgene	FlyBase_FBst0471360
UAS-Tmem63-RNAi	RNAi transgene	FlyBase_FBst0470667
UAS-TMCO1-RNAi	RNAi transgene	BDSC_42896
UAS-TMCO1-RNAi	RNAi transgene	BDSC_55909
UAS-TrpA1-RNAi	RNAi transgene	BDSC_66905
UAS-Trpm-RNAi	RNAi transgene	BDSC_31291
UAS-Trpml-RNAi	RNAi transgene	BDSC_31294
UAS-wtrw-RNAi	RNAi transgene	BDSC_51563

Table S2. Larval behaviors scored in this study

Behavior	Description / Criteria
Locomotion	Continuous forward movement with smooth, regular peristalsis
Pausing	Break in locomotion, lasting less than 1 second
Freezing	Break in locomotion that persists for longer than 1 second
Hunching	Contraction along the anterior-posterior axis; no forward / backward motion or curling
Backward locomotion	Anterior-to-posterior peristalsis accompanied by movement in reverse
Writhing crawl	Forward movement with anterior and posterior sweeping of the body, tilting onto the side axis
C-bending	Bending into a c-shape, with both head and tail bending in the same direction; includes incomplete rolls
Rearing	Upwards bending or arching of anterior part of the body, with posterior part largely stationary
Rolling	Larva completes a full 360-degree rotation of its body

Table S3. Solutions used in calcium imaging studies.

HL3.1, *Drosophila* saline			
Compound	**M.W. (g/mol)**	**1X Concentration (mM)**	**For 1L (1X)**
NaCl	58.44	120	7.013 g
KCl	74.55	5	0.373 g
Proline	115.13	5	0.576 g
HEPES	238.30	10	2.383 g
Trehalose	378.33	5	3.78 g
Sucrose	342.30	32.5	11.125 g
CaCl2	1M stock	1.5	1.5 ml from 1M stock
MgCl2	1M stock	1	1 ml from 1M tock
		pH (with NaOH)	7.15
		Osmolarity (mOsm/L)	310

Zero Ca2+ / EGTA HL3.1			
Compound	**M.W. (g/mol)**	**1X Concentration (mM)**	**For 1L (1X)**
NaCl	58.44	120	7.013 g
KCl	74.55	5	0.373 g
Proline	115.13	5	0.576 g
HEPES	238.30	10	2.383 g
Trehalose	378.33	5	3.78 g
Sucrose	342.30	32.5	11.125 g
EGTA	380.35	1.5	0.571 g
MgCl2	1M stock	1	1 ml from 1M tock
		pH (with NaOH)	7.15
		Osmolarity (mOsm/L)	310

20mM Ca2+ HL3.1			
Compound	**M.W. (g/mol)**	**1X Concentration (mM)**	**For 1L (1X)**
NaCl	58.44	101.5	5.932 g
KCl	74.55	5	0.373 g
Proline	115.13	5	0.576 g
HEPES	238.30	10	2.383 g
Trehalose	378.33	5	3.78 g
Sucrose	342.30	32.5	11.125 g
CaCl2	1M stock	20	20 ml from 1M stock
MgCl2	1M stock	1	1 ml from 1M tock
		pH (with NaOH)	7.15
		Osmolarity (mOsm/L)	310

Isotonic (modified from *Drosophila* saline to maintain ionic balance across osmolarities)			
Compound	**M.W. (g/mol)**	**1X Concentration (mM)**	**For 1L (1X)**
NaCl	58.44	90	5.260 g
KCl	74.55	5	0.373 g
Proline	115.13	5	0.576 g
HEPES	238.30	10	2.383 g
Trehalose	378.33	5	3.78 g
Sucrose	342.30	92.5	31.663 g
CaCl2	1M stock	1.5	1.5 ml from 1M stock
MgCl2	1M stock	1	1 ml from 1M tock
		pH (with NaOH)	7.15
		Osmolarity (mOsm/L)	310

85% Hypoosmotic			
Compound	**M.W. (g/mol)**	**1X Concentration (mM)**	**For 1L (1X)**
NaCl	58.44	90	5.260 g
KCl	74.55	5	0.373 g
Proline	115.13	5	0.576 g
HEPES	238.30	10	2.383 g
Trehalose	378.33	5	3.78 g
Sucrose	342.30	46.5	15.917 g
CaCl2	1M stock	1.5	1.5 ml from 1M stock
MgCl2	1M stock	1	1 ml from 1M tock
		pH (with NaOH)	7.15
		Osmolarity (mOsm/L)	

70% Hypoosmotic			
Compound	**M.W. (g/mol)**	**1X Concentration (mM)**	**For 1L (1X)**
NaCl	58.44	90	5.260 g
KCl	74.55	5	0.373 g
Proline	115.13	5	0.576 g
HEPES	238.30	10	2.383 g
Trehalose	378.33	5	3.78 g
Sucrose	342.30	0	15.917 g
CaCl2	1M stock	1.5	1.5 ml from 1M stock
MgCl2	1M stock	1	1 ml from 1M tock
		pH (with NaOH)	7.15
		Osmolarity (mOsm/L)	